# NUMERICAL SIMULATION OF INTERNAL HEAT GENERATION AND ABSORPTION ON MAGNETOHYDRODYNAMIC MIXED CONVECTION HEAT TRANSFER IN AN ENCLOSURE HAVING VARIABLE UNDULATION IN VERTICAL WALLS
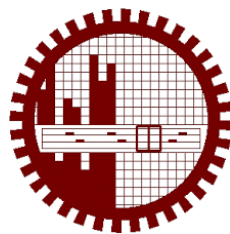
Thesis submitted for the award of the degree of

**Master of Philosophy**

at the Bangladesh University of Engineering and Technology

by

Rajib Kumar Bhowmik

Student No. 1017093003P

Registration No. 1017093003, Session: October, 2017

Department of Mathematics

Bangladesh University of Engineering and Technology (BUET),

Dhaka-1000, Bangladesh

September- 2022

The thesis entitled **"NUMERICAL SIMULATION OF INTERNAL HEAT GENERATION AND ABSORPTION ON MAGNETOHYDRODYNAMIC MIXED CONVECTION HEAT TRANSFER IN AN ENCLOSURE HAVING VARIABLE UNDULATION IN VERTICAL WALLS"**, submitted by Rajib Kumar Bhowmik, Student No. 1017093003P, Registration No. 1017093003, Session October, 2017 has been accepted as satisfactory in partial fulfillment of the requirement for the degree of Master of Philosophy in Mathematics on 25th September 2022.

## BOARD OF EXAMINERS

1. _____

   **Dr. Md. Manirul Alam Sarker**                    Chairman
   Professor                                          (Supervisor)
   Department of Mathematics, BUET, Dhaka-1000

2. _____

   ~~Dr. Farid Uddin Ahmed~~ Dr. Khandken Farid Uddin Ahmed    Member
   Professor                                          (Ex-Officio)
   Department of Mathematics, BUET, Dhaka-1000

3. _____

   **Dr. Md. Abdul Hakim Khan**                       Member
   Professor
   Department of Mathematics, BUET, Dhaka-1000

4. _____

   **Dr. Nazma Parveen**                              Member
   Professor
   Department of Mathematics, BUET, Dhaka-1000

5. _____

   **Dr. Ujjwal Kumar Deb**                           Member
   Professor                                          (External)
   Department of Mathematics, CUET

## AUTHOR'S DECLARATION

I hereby announce that the work which is being presented in this thesis entitled **"NUMERICAL SIMULATION OF INTERNAL HEAT GENERATION AND ABSORPTION ON MHD MIXED CONVECTION HEAT TRANSFER IN AN ENCLOSURE HAVING VARIABLE UNDULATION IN VERTICAL WALLS"** submitted in partial fulfillment of the requirements for the decoration of the degree of Master of Philosophy, Department of Mathematics, BUET, Dhaka, is an authentic record of my own work.

The object presented in this thesis has not been submitted by me for the award of any other degree in this university or any other university.
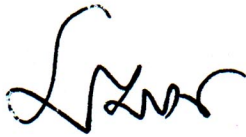
**(Rajib Kumar Bhowmik)**

Date: 25th September, 2022

# CERTIFICATE OF RESEARCH

This is to certify that the work presented in this thesis is carried out by the author under the supervision of Dr. Md. Manirul Alam Sarker, Professor, Department of Mathematics, Bangladesh University of Engineering & Technology, Dhaka-1000, Bangladesh.

-------------------------------------------------

**Prof. Dr. Md. Manirul Alam Sarker**

**Supervisor**

--------------------------------------

**Rajib Kumar Bhowmik**

**Dedicated
To**

**My Family**

# ACKNOWLEDGEMENT

# ABSTRACT

Mixed convection heat transfer performance in presence of a magnetic field in an enclosure having variable undulation in vertical walls under the impact of internal heat generation and absorption has been studied numerically in this thesis. The governing equation consisting of a set of non-linear differential equations in this Magneto-hydrodynamic (MHD) mixed convection problem is intrinsically non-linear as well as coupled.

The investigations are conducted for different values of Reynolds number $(0.1 \leq Re \leq 10)$, Grashof number $(10^3 \leq Gr \leq 10^6)$, Richardson number $(0.1 \leq Ri \leq 10)$, Undulations number $(1 \leq \lambda \leq 3)$, heat absorption and generation $(-6 \leq \Delta \leq 6)$ but for fixed amplitude with $Ha = 20$ whereas Prandtl number is kept constant at 0.70. Various characteristics such as streamlines, isotherms and heat transfer rate in terms of the average Nusselt number $(Nu_{av})$ and average fluid temperature $(\theta_{av})$ are presented for the aforementioned parameters.

The results indicate that the mentioned parameters strongly affect the flow phenomenon and temperature field inside the wavy cavity. It may be claimed that, heat transfer performance could be enhanced 3.8% for heat absorption to heat generation. The results of this study conformed very well with the published ones.

# TABLE OF CONTENTS

| Items | Page |
|---|---|

# NOMENCLATURE

| | |
|---|---|
| $A$ | amplitude |
| $B_0$ | magnetic induction (Wb/m$^2$) |
| $C_p$ | specific heat at constant pressure (J/kg.K)dfin position |
| g | gravitational acceleration (ms$^{-2}$) |
| $h*$ | convective heat transfer coefficient (W/m$^2$.K) |
| $Ha$ | Hartmann number |
| k | thermal conductivity of fluid (Wm$^{-1}$K$^{-1}$) |
| n | dimensional distance either along x or y direction (m) |
| $N$ | dimensionless distance either along X or Y direction |
| $Nu_{av}$ | average Nusselt number |
| $Nu_L$ | local Nusselt number |
| p | pressure |
| $P$ | dimensionless pressure $(pw^2 / \rho\alpha^2)$ |
| $Pr$ | Prandtl number |
| $Re$ | Reynolds number |
| $Ri$ | Richardson number |
| $T$ | dimensional fluid temperature (K) |
| $\Delta T$ | dimensional temperature difference (K) |
| u | velocity in x-direction (m/s) |
| $U$ | dimensionless horizontal velocity |
| v | velocity in y-direction (m/s) |
| $V$ | dimensionless vertical velocity |
| $W$ | enclosure width and height |
| x, y | Cartesian coordinates (m) |
| X, Y | dimensionless Cartesian coordinates |

## Greek Symbols

| | |
|---|---|
| $\alpha$ | thermal diffusivity ($m^2s^{-1}$) |
| $\beta$ | coefficient of thermal expansion ($K^{-1}$) |
| $\lambda$ | number of undulations |
| $\theta$ | dimensionless fluid temperature |
| $\mu$ | dynamic viscosity of the fluid ($m^2s^{-1}$) |
| $v$ | kinematic viscosity of the fluid ($m^2s^{-1}$) |
| $\rho$ | density of the fluid ($kgm^{-3}$) |
| $\sigma$ | fluid electrical conductivity ($\Omega^{-1}.m^{-1}$) |

## Subscripts

| | |
|---|---|
| av | average |
| c | cold |
| $h$ | hot |

# LIST OF TABLES

# LIST OF FIGURES

## 1.1 INTRODUCTION

The phenomenon of heat transfer was known to human being even in the primitive age when they used to use solar energy as a source of heat. Heat transfer in its initial stage was conceived with the invention of fire in the early age of human civilization. Since then, its knowledge and use has been progressively increasing each day as it is directly related to the growth of human civilization. With the invention of stream engine by James's watt in 1765 A. D., the phenomenon of heat transfer got its first industrial recognition and after that its use extended to a great extent and spread out in different spheres of engineering fields. In the past three decades, digital computers, numerical techniques and development of numerical models of heat transfer have made it possible to calculate heat transfer of considerable complexity and thereby create a new approach to the design of heat transfer equipment.

## 1.2 MODES OF HEAT TRANSFER

Heat transfer is the process of transportation of thermal energy form one system to another as a result of temperature difference. The transfer of energy is always from the higher temperature medium to the lower temperature one and heat transfer stops when the two mediums reach the same temperature. Heat can be transferred in three different mechanism or modes: conduction, convection, and radiation. All modes of heat transfer require the existence of temperature difference, and all modes are from the high temperature medium to a lower temperature one. In reality the combined effect of these three modes of heat transfers control temperature distribution in a medium. Detailed discussion of the three modes of heat can be found in Cengel [5]. Brief descriptions of convection, conduction, and radiation modes are given below:

### 1.2.1 Convection

Convection is the mode of energy transfer between a solid surface and the adjacent liquid or gas that is in motion, and it involves the combined effects of conduction and fluid motion. The faster the fluid motion, the greater the convection heat transfers. In the absence of any bulk fluid motion, heat transfer between a solid surface and the adjacent fluid is by pure conduction. The presence of bulk motion of the fluid enhances the heat transfer between the solid surface and the fluid, but it also complicates the determination of heat transfer rates. The convective heat transfer bifurcates into two branches; the natural convection and forced convection.

Convection is called forced convection if the fluid is forced to flow over the surface by external means such as a fan, pump, or the wind. In contrast, convection is called natural (or free) convection if the fluid motion is caused by buoyancy forces that are induced by density differences due to the variation of temperature in the fluid. Buoyancy is due to the combined presence of the fluid density gradient and body force.

### 1.2.2 Conduction
Conduction is the transfer of energy from the more energetic particles of a substance to the adjacent less energetic ones as a result of interactions between the particles. Conduction can take place in solids, liquids, or gasses. The rate of heat conduction through a medium depends on the geometry of the medium, its thickness, and the material of the medium, as well as the temperature difference across the medium.

### 1.2.3 Radiation
Radiation is the energy emitted by matter in the form of electromagnetic waves (or photons) as a result of the changes in the electronic configurations of the atoms or molecules. Unlike conduction and convection, the transfer of energy by radiation does not require the presence of an intervening medium. All materials radiate thermal energy based on their temperature. The hotter an object, the more it will radiate. In fact, energy transfer by radiation is fastest (at the speed of light) and it suffers no attenuation in a vacuum. This is how the energy of the sun reaches the earth.

### 1.3 SOME USEFUL DEFINITIONS
Some useful definitions related to the present study are discussed below. Detailed discussion of these definitions can be found in Cengel and Cimbala [2].

### 1.3.1 Viscosity
The viscosity of a fluid which is a strong function of temperature is a measure of its resistance to deformation. A friction force develops between two adjacent fluid layers while they move relative to each other and the slower layer tries to slow down the faster layer. This type of internal resistance to flow is quantified by the fluid therefore no fluid is of zero viscosity. As temperature increases, the viscosity of liquids decreases whereas the viscosity of gases increases with temperature.

### 1.3.2 Viscous Flow

Such flows are called viscous whose flow patterns are dominated by the viscous properties of the fluid. This arises in fluids where the velocity gradients are comparatively large. The flow close to the walls of the pipes can be treated as viscous flows.

### 1.3.3 Newtonian Fluid

Newtonian fluids are those fluids for which the constant of proportionality i.e., the coefficient of viscosity ($\mu$) does not change with the rate of deformation. In other words, fluids that follow Newton's law of viscosity are known as Newtonian fluids.

### 1.3.4 Compressible and Incompressible Flow

Compressible flow means a flow that undergoes a notable variation in density with trending pressure. That is, a compressible flow is one in which the density varies in the different portion of the fluids. Incompressible flow refers to the fluid flow in which the fluid's density is constant. For a density to remain constant, the control volume has to remain constant.

Even though the pressure changes, the density will be constant for an incompressible flow. Incompressible flow means flow with variation of density due to pressure changes is negligible or infinitesimal. All the liquids at constant temperature are incompressible. The behavior of control volume (CV) for incompressible and compressible flow is depicted in the image below. It can be seen that the control volume remains constant for a flow that is incompressible and CV is squeezed for compressible flow.

### 1.3.5 Thermal Conductivity

Thermal conductivity is defined as the quantity of heat ($Q$) transmitted through a unit thickness ($L$) in a direction normal to a surface of unit area ($A$) due to a unit temperature gradient ($\Delta T$) under steady state conditions and when the heat transfer is dependent only on the temperature gradient Çengel and Yunus [4]. That is,

$$\text{Thermal Conductivity} = \frac{heat \times distance}{area \times temperature\ gradient}$$

$$= \frac{Q \times L}{A \times \Delta T}$$

### 1.3.6 Thermal Diffusion

Thermal diffusion is a relative motion of the components of a gaseous mixture or solution, which is established when there is a temperature gradient in a medium. Thermal diffusion in liquids has an alternative term, the Soret effect, named after the Swiss scientist, who

3

investigated thermal diffusion in solutions in 1879–1881. Thermal diffusion in gases was theoretically predicted by Chapman and Enskog (1911–1917) on the basis of the kinetic theory of gases, and it was later discovered experimentally by Chapman and Dutson in 1917. Thermal diffusion disturbs the homogeneity of mixture composition: the concentration of components in the regions of increased and decreased temperatures, respectively, becomes different. Since the establishment of a concentration gradient causes, in turn, ordinary diffusion, in a stationary nonuniform temperature field a steady state inhomogeneous state is possible in which the separation effect of thermal diffusion is balanced by the counteraction of concentration diffusion.

$$\text{Thermal diffusion, } \alpha = \frac{\kappa}{\rho c_p}$$

Where,

$\kappa = $ is thermal conductivity

$\rho = $ is density

$c_p = $ is specific heat capacity

### 1.3.7 Free and Force Convection

In this studies related to heat transfer considerable effort has been directed towards the convective mode in which the relative motion of the fluid provides an additional mechanism mode for the transfer of energy and material the latter being a more important consideration in cases where mass transfer due to a concentration difference occurs Convection is inevitably coupled with the convective mechanisms since although the fluid motion modifies the transport process the eventual transfer of energy from one fluid element to another in its predominantly that of conduction because the relative fluid motion is brought to zero at the surface. A study of convective heat transfer therefore involves the mechanisms of conduction and sometimes those of radioactive processes as well coupled with that fluid flow.

The heat transfer in convective mode is divided into two basic processes If no externally induced flow is provided and flow arises naturally simply owing to the effect of a density difference resulting from a temperature or concentration difference in a body force field such as the gravitational field the process is referred to the natural convection On the other hand if the motion of the fluid is caused by an external agent as the externally imposed hand if the motion of the fluid is caused by an external agent such as the externally imposed flow of a fluid stream over a heated object the process is termed as force convection. In the force convection the fluid flow may be the result of instance a fan a blower the wind or the motion

of the heated object itself Such problems are very frequently encountered in technology where the heat transfer to or from body is often due to an imposed flow of a fluid at a different temperature from that of body. On the other side in the natural convection the density difference gives rise to buoyancy effects owing to which the flow is generated. A heated body cooling in ambient air generates such a flow in the region surrounding it. Similarly, the buoyant flow to arising from heated rejection to the atmosphere and to other ambient media circulation arising in heated rooms in the atmosphere and in bodies of water rise of buoyant flow to cause thermal stratification of the medium as in temperature inversion and many other such heat transfer process in our natural environment as well as in many technological applications are included in the area of natural convection. The flow may also arise owing to concentration difference such as those caused by salinity difference in the sea and by composition difference in chemical processing unit and these cause a natural convection mass transfer more available in Shercliff [3].

### 1.3.8 Mixed convection

Practically some time both processes natural and force convection are important and heat transfer is by mixed convection in which neither mode is truly predominant. The main difference between the really lies in the word external. A heated body lying in still air loses energy by natural convection. But it also generates a buoyant flow above it and body placed in that flow is subjected to an external flow and it becomes necessary to determine the natural as well as the forced convection effects and the regime in which the heat transfer mechanisms lie.

When the study of magneto-hydrodynamics become a popular subject, it was normal that these flows would be investigated with the additional ponder motive body forces as well as the buoyancy force. At a first glance there seems to be practical applications for these MHD solutions, for most heat exchanger utilizes liquids, whose conductively is so small that prohibitively large magnetic fields are necessary to influence the flow. But some nuclear power plants employ heat exchange with liquid metal coolants, so the applications of moderate magnetic fields to change the convection pattern appears feasible. Another classical natural convection problem is the thermal instability that occurs in a liquid heated from below. This subject is of natural interest to geophysicists and astrophysics, although some applications might arise in boiling heat transfer.

## 1.4 DIMENSIONLESS PARAMETERS

### 1.4.1 Reynold's Number ($Re$)

Reynolds related the inertia to viscous forces and arrived at a dimensionless parameter.

$$Re = \frac{\text{Inertia Force}}{\text{Viscous Force}}$$

$$= \frac{\text{Mass} \times \text{Acceleration}}{\text{Shear Stress} \times \text{Cross Sectional Area}}$$

$$= \frac{\rho L^3 \times LT^{-2}}{\mu U L^{-1} \times L^2}$$

$$= \frac{\rho L^2 U^2}{\mu U L}$$

$$\text{Re} = \frac{UL}{\nu},$$

Where $U, L, \rho \ and \ \mu$ are the characteristic values of velocity, length density and coefficient of the viscosity of the fluid respectively. Also $\nu = \frac{\mu}{\rho}$ is the kinematic viscosity.

If an airplane wing needs testing, one can make a scaled down model of the wing and test it in a wind tunnel using the same Reynolds number that the actual airplane is subjected to. If for example the scale model has linear dimensions one quarter of full size, the flow velocity of the model would have to be multiplied by a factor of 4 to obtain similar flow behavior. Alternatively, tests could be conducted in a water tank instead of in air (provided the compressibility effects of air are not significant). As the kinematic viscosity of water is around thirteen times less than that of air at $15 \ °C$, in this case the scale model would need to be about one thirteenth the size in all dimensions to maintain the same Reynolds number, assuming the full-scale flow velocity was used. The results of the laboratory model will be similar to those of the actual plane wing results. Thus, there is no need to bring a full-scale plane into the lab and actually test it. This is an example of "dynamic similarity". Reynolds number is important in the calculation of a body's drag characteristics. A notable example is that of the flow around a cylinder. Above roughly $3 \times 10^6$, $Re$ the drag coefficient drops considerably. This is important when calculating the optimal cruise speeds for low drag (and therefore long range) profiles for airplanes.

Where the viscosity is naturally high, such as polymer solutions and polymer melts, flow is normally laminar. The Reynolds number is very small and Stokes' Law can be used to measure the viscosity of the fluid. Spheres are allowed to fall through the fluid and they reach the

terminal velocity quickly, from which the viscosity can be determined. The laminar flow of polymer solutions is exploited by animals such as fish and dolphins, who exude viscous solutions from their skin to aid flow over their bodies while swimming. It has been used in yacht racing by owners who want to gain a speed advantage by pumping a polymer solution such as low molecular weight polyoxymethylene in water, over the wetted surface of the hull. It is however, a problem for mixing of polymers, because turbulence is needed to distribute fine filler (for example) through the material. Inventions such as the "cavity transfer mixer" have been developed to produce multiple folds into a moving melt so as to improve mixing efficiency. The device can be fitted onto extruders to aid mixing. More details are available in Çengel and Yunus [4].

### 1.4.2 Prandtl number ($Pr$)

The Prandtl number is the ratio of kinematic viscosity to thermal diffusivity and may be written as follows,

$$Pr = \frac{\text{Kinematic Viscosity}}{\text{Thermal Diffusivity}}$$

$$= \frac{C_p \mu}{\kappa}$$

where $C_p$ is the specific heat at constant pressure and $\kappa$ is the thermal conductivity. The value of $\nu = \frac{\mu}{\rho}$, Kinematic Viscosity. Thus, the Prandtl number shows that the relative importance of heat conduction and viscosity of a fluid.

Evidently, the value of $Pr$ varies from fluid to fluid. For air at $20^0$c, $Pr = 0.71$ (approx.), for water at $20^0$c, $Pr = 0.70$ (approx.), for mercury at $20^0$c, $Pr = 0.44$ (approx.) but for high viscous fluid it very large e.g., for glycerin at $20^0$c, $Pr = 7250$. More details are available in Çengel and Yunus [4].

### 1.4.3 Magnetic Parameter ($M$)

This is obtained from the magnetic force to the inertia force and is defined as

$$M = \frac{\text{Magnetic Force}}{\text{Inertia Force}}$$

$$= \frac{\sigma L \mu_e B_0^2}{\rho U}$$

Where $\mu_e$ is the magnetic permeability, $\sigma$ is the electrical conductivity, $B_0$ be the constant induced magnetic field.

### 1.4.4 Grashof Number ($Gr$)

The flow regime in free convection is governed by the dimensionless Grashof number, which represent the ratio of the buoyancy force to the viscous forces acting on the fluid, and is defined as

$$Gr = \frac{g\beta L^3 (T_w - T_\infty)}{\vartheta^2},$$

Where $g$ is the acceleration due to gravity, $\beta$ is the volumetric thermal expansion coefficient, $T_w$ is the wall temperature, $T_\infty$ is the ambient temperature, $L$ is the characteristic length and $\vartheta$ is the kinematics viscosity. The Grashof number $Gr$ plays same role in free convection as the Reynolds number $Re$ plays in forced convection. As such, the Grashof number provides the main criterion in determining whether the fluid flow is laminar or turbulent in free convection. For vertical plates, the critical value of the Grashof number is observed to be about $10^9$, the flow regime on a vertical plate becomes turbulent at Grashof numbers greater than $10^9$. More details are available in Çengel and Yunus [4].

### 1.4.5 Richardson Number ($Ri$)

Richardson number represents the importance of natural convection relative to the forced convection. The Richardson number in this context is defined as

$$Ri = \frac{g\beta (T_{hot} - T_{ref})}{v^2},$$

Where $g$ is the gravitational acceleration, $\beta$ is the thermal expansion coefficient, $T_{hot}$ is the hot wall temperature, $T_{ref}$ is the reference temperature, $L$ is the characteristic length, and $\vartheta$ is the characteristic velocity. The Richardson number can also be expressed by using a combination of the Grashof number and Reynolds number,

$$Ri = \frac{Gr}{Re^2}.$$

Typically, the natural convection is negligible when $Ri < 0.1$, forced convection is negligible when $Ri > 10$, and neither is negligible when $0.1 < Ri < 10$. It may benoted that usually, the forced convection is large relative to natural convection exceptin the case of extremely low forced flow velocities. However, buoyancy often plays asignificant role in defining the laminar-turbulent transition of a mixed convection flow. In the design of water filled thermal energy storage tanks, theRichardson number can be useful by Çengel and Cimbala [2].

### 1.4.6 Hartmann Number, $Ha$

Hartmann number is the ratio of electromagnetic force to the viscous force first introduced by Hartmann. It is defined by:

$$Ha = B_0 L \sqrt{\frac{\sigma}{\mu}},$$

Where, $B_0$ is the magnetic field, $L$ is the characteristic length scale, $\sigma$ is the electrical conductivity, μ is the viscosity. In addition, it is a dimensionless quantity characterizing flow of conducting fluid in a transverse magnetic field, being the product of the magnetic flux density, a representative length, and the square root of the ratio of electrical conductivity to viscosity. More details are available in Çengel and Yunus [2].

### 1.5 MAGNETO-HYDRODYNAMIC (MHD)

Magneto-hydrodynamic (MHD) is a branch of magneto fluid dynamics i.e., continuum mechanics, which deals with the flow of electrically conducting fluids in electric and magnetic fields. The largest advance towards an understanding of such phenomena probably comes from the field of astrophysics. It has long suspected that and much of the matter in the universe is in the plasma or highly ionized gaseous state and much of the basic knowledge in the area of electromagnetic fluid dynamics evolved from these studies. The field of Magneto-hydrodynamics consists of the study of a continuous, electrically conducting fluid under the influence of electromagnetic fields as a branch of plasma physics. Originally, MHD included only the study of strictly incompressible fluid but today the terminology is applied to studies of partially ionized gases as well as other names have been suggested such as magneto-fluid-mechanics or magneto-aero-dynamics, but original nomenclature has persisted. The essential requirement for problems to be analyzed under the laws of MHD is that the continuous approach be applicable.

There are many natural phenomena and engineering problems are susceptible to MHD analysis, it is useful astrophysics because much of the universe is filled with widely spaced charged particles and permeated by magnetic fields and so the continuum assumption becomes applicable. Geophysicist's encounter MHD phenomena in the interaction of conducting fluids and magnetic fields that are present in around heavenly bodies. Engineers employ MHD principles in the design of heat exchange, pumps and flow-meters, in space vehicle propulsion, control and re-entry problem, in designing communications and radar system, in creating novel power generating systems and in developing confinement schemes for controlled fusion.

The most important application of MHD of electrical power with the flow of an electrically conducting fluid through a transverse magnetic field. Recently experiments with ionized gases have been performed with the hope of producing power on a large scale in stationary plants with large magnetic fields. Cryogenic and super conducting magnets are required scale is of interested for space for space application. Generally, it is known that several intermediate transformations are necessary to convert the heat energy into electrity. Each of these steps mean a loss of energy. This naturally limits the overall efficiency reliability and compactness of the convention process. Methods for direct conversion to energy are now increasingly receiving attentions. Of these, the fuel cell converts the chemical energy of fuel directly into electrical energy, fusion energy utilizes the energy released when two hydrogen nuclei fuel into a heavier one and thermo-electrical power generation uses a thermocouple, Magneto-hydrodynamics power generation is another important new process that is receiving worldwide attention.

In the experiment of Faraday (1832), the principle MHD effects were first demonstrated He discovered that a voltage was induced across the tube due to the motion of the mercury across the magnetic fields perpendicular to the direction of flow and the magnetic field by the experiment of the flow of mercury in glass tubes places between poles of a magnet. Faraday also suggested that electrical power could be generated in a load circuit by the interaction of a flowing conducting fluid and a magnetic field. Alfven (1942) discovered MHD waves in the sun. Theses waves are produced by disturbance which propagate simultaneously in the conducting fluid and the magnetic field. The analogy that explains the generation of an Alfven wave is that of a harp string plucked while submerged in a fluid. The string provides elastic force and the fluid provides inertia force and they combine to propagate a perturbing wave through the fluid and the string.

In summary MHD phenomena result from the mutual effect of a magnetic field and conducting fluid flowing across it. Thus, an electromagnetic force is produced in a fluid flowing across a transverse magnetic field. Field combines to produce a force that resists the fluids motion. The current also generates its own magnetic fields which distorts the original magnetic field. An opposing or pumping force on the fluid can be produced by applying an electric field perpendicularly to the magnetic field. Disturbance in either the magnetic field or the fluid can propagate in both to produce MHD waves as well as upstream and downstream wave phenomena. The science of magneto-hydrodynamics is the detailed study of these phenomena, which occur in nature and are produced in engineering devices.

## 1.6 MHD AND HEAT TRANSFER

With the advent of hyper sonic flight, the field of MHD as defined above which has attracted the interests of aero dynamics and associated largely with liquid metal pumping. It is possible to alter the flow and the heat transfer around high velocity vehicles provided that the air is sufficiently ionized. Furthermore, the invention of high temperature facilities such as the shock tube plasma jet has provided laboratory sources of ionized, gas. As a result of this many of the classical problem of fluid mechanics have been reinvestigate. Some of these analyses awake out of the natural tendency of scientists to search a new subject. In this case it was the academic problem of solving the equation of fluid mechanics with a new body force and another source of dissipation in the energy equation. Sometimes there was no practical application for these results, as for example natural convection MHD flows have been of interest to the engineering community only since the investigations directly apply to the problems in geophysics and astrophysics. But it was in the field of aerodynamics heating that the largest interest was awaked.

## 1.7 MIXED CONVECTION HEAT TRANSFER IN CAVITY

Mixed convection in cavity is a topic of contemporary importance, because cavity filled with fluid are central components in a long list of engineering and geophysical systems. The flow and heat transfer induced in an enclosure differs fundamentally from the external mixed convection boundary layer. Mixed convection in a cavity, like the external mixed convection boundary layer that is caused by the heat transfer interaction between a single wall and a very large fluid reservoir is the result of the complex interaction between finite size fluid systems in thermal communication with all the walls that confine it. The complexity of this internal interaction is responsible for the diversity of flows that can exist inside enclosure. The phenomenon of mixed convection in cavity is varied by the geometry and the orientation of the enclosure. Judging by the potential engineering applications, the enclosure phenomena can loosely be organized into two classes such as vented cavity and lid-driven cavity.

In a vented cavity, where the interaction between the external forced stream provided by the inlet and the buoyancy driven flows induced by the heat source leads to the possibility of complex flows. Therefore, it is important to understand the fluid flow and heat transfer characteristics of mixed convection in a vented cavity.

On the other hand, the fluid flow and heat transfer in a lid-driven cavity where the flow is induced by a shear force resulting from the motion of a lid combined with the buoyancy force

due to non-homogeneous temperature of the enclosure wall, provides another problem, studied extensively by researchers to understand the interaction between buoyancy and shearing forces in such flow situation. The interaction between buoyancy driven and shear driven flows inside a closed cavity in a mixed convection regime is quite complex. Therefore, it is also important to understand the fluid flow and heat transfer characteristics of mixed convection in a lid-driven cavity.

## 1.8 LITERATURE REVIEW

Mixed convection flow and heat transfer in an enclosure has become important in several industrial, scientific and engineering fields. In astrophysical and geophysical studies, the MHD mixed convection flows of an electrically conducting fluid have also vast application. Many researchers studied the MHD mixed convection flow in an enclosure for the applications in the branch of science and technology such as in the field of mechanical engineering and chemical engineering. MHD heat transfer has great importance in the liquid metal flows, ionized gas flow in a nuclear reactor and electrolytes. Research works on the effect of internal heat generation and absorption on magnetohydrodynamic mixed convection heat transfer in an enclosure are very limited, though these have many modern applications viz missile technology used in army, nuclear power plant, parts of aircraft and ceramic tiles, the heat radiation and chemical reaction with or without magnetic field, suction injection has been analyzed by several characters.

Ismael *et al.* investigated mixed convection in a lid-driven square cavity with partial slip. Regardless of Richardson number ranges and beyond its critical value, the partial slip parameter offers no effect on the convection heat transfer inside the cavity. Slip effect in the mixed convection is the dominance one over the natural convection. Mahmud *et al.* [9] numerically studied the free convection in an enclosure with vertical wavy walls. For a constant Grashof number and aspect ratio, heat transfer falls gradually with an increase of surface waviness up to a certain value of surface waviness, above which heat transfer increases again. Nada and Chamkha [10] carried out a parametric study of the governing parameters such as the Richardson number, bottom wall geometry ratio and the nanoparticles volume fraction is conducted and a representative set of graphical results is presented and discussed to illustrate the effects of these parameters on the flow and heat transfer characteristics. It is found that the presence of nanoparticles causes significant heat transfer augmentation for all values of Richardson numbers and bottom wall geometry ratios. Saha *et al.* [11] has done a numerical

study on mixed convection heat transfer in a lid-driven cavity with a wavy bottom surface. They observed that wavy lid-driven cavity can be considered as an effective heat transfer mechanism at larger wavy surface amplitudes and higher Grashof number.

Rahman *et al.* [12] studied numerically the opposing mixed convection in a vented enclosure. They found that with the increase of Reynolds and Richardson numbers the convective heat transfer becomes predominant over the conduction heat transfer and showed that the rate of heat transfer from the heated wall is significantly depended on the position of the inlet port. Recently, Asad *et al.* [13] have analyzed the impact of a closed space rectangular heat source on natural convective flow through triangular cavity. Singh and Sharif [14] extended their works by considering six placement configurations of the inlet and outlet of a differentially heated rectangular enclosure whereas the previous work was limited to only two different configurations of inlet and outlet. Moallemi and Jang [15] studied two-dimensional laminar flow and effects of small to moderate Prandtl numbers on the flow and the heat transfer in the cavity are investigated for different values of Richardson number. The temperature and the flow fields in the cavity are calculated and presented to illustrate the strong influence of Prandtl number. Gau *et al.* [16] performed experiments on mixed convection in a horizontal rectangular channel with side heating. Hsu and Wang [17] investigated the mixed convective heat transfer where the heat source was embedded on a board mounted vertically on the bottom wall at the middle in the enclosure. Amiri *et al.* [18] investigated the effect of sinusoidal wavy bottom surface on mixed convection heat transfer in a lid-driven cavity. They investigated the effect of Richardson number, undulation number and amplitude of the wavy surface on flow structure and heat transfer characteristics. Wang and Jaluria [19] numerically investigated the characteristics of the instability and the resulting effect on the heat transfer in mixed convection flow in a horizontal duct with discrete heat sources. Very recently, Oztop [20] studied the influence of exit opening location on mixed convection in a channel with volumetric heat sources using finite volume method. A. B. Nakhi *et al.* [21] has focused on the numerical study of steady, laminar, conjugate natural convection in a square enclosure with an inclined thin fin of arbitrary length. It was found that the thin fin inclination angle and length, and solid-to-fluid thermal conductivity ratio have significant effects on the local and average Nusselt number at the heated surfaces of the enclosure fin system. Sertel and Bilen [22] studied on the effect of using sinusoidal profile in fins on thermal performance. Elatar *et al.* [23] conducted a numerical study for laminar natural convection inside a square enclosure with a single horizontal fin attached to its hot wall. They concluded that fin efficiency is suppressed by

increasing the fin length and the rate of fin efficiency increases with the decrease and the fin effectiveness is enhanced by increasing the values of Rayleigh numbers. It is also found that in general, the fin effectiveness increases with the increase of the fin length. Asad *et. al.* [24] carried a numerical investigation of Natural Convection Flow in a Hexagonal Enclosure Having Vertical Fin. Angirasa [25] numerically studied and explained the complex interaction between buoyancy and forced flow in a square enclosure with an inlet and a vent situated respectively, at the bottom and top edges of the vertical isothermal surface, where the other three walls were adiabatic. Cheng and Chen [26] investigated the effects of inclination on buoyancy induced flow oscillation in a lid-driven arc-shaped cavity. Alam and Tunç [27] introduced an analytical method for solving exact solutions of the nonlinear Bogoyavlenskii equation and the nonlinear diffusive predator–prey system. Ahmad *et. al.* [28] studied analytic approximate solutions for some nonlinear Parabolic dynamical wave equations. Taylor and Hood [29] numerically solved the Navier-Stokes equations using finite element technique.

Magnetic field effect of electrically conducting fluid on the heat transfer and fluid flow encountered in many engineering applications such as coolers of nuclear reactors, Magnetohydrodynamics (MHD) power generators, micro MHD pumps, and liquid metal flow control, etc. Javaherdeh *et al.* [30] carried an investigation on natural convection of nanofluid in a wavy cavity in the presence of magnetic field on variable heat surface temperature. The results show that in the presence of the magnetic field the local Nusselt number decreases at the hot wall. Moreover, the enhancement in the heat transfer performance increases with an increasing nanoparticle concentration. However, for all values of Rayleigh number, the presence of nanoparticles leads to significant enhancement in heat transfer and the increase of Rayleigh number causes the heat transfer mechanism to change from conduction to convection. Malleswaran and Sivasankaran [31] done a numerical simulation on MHD mixed convection in a lid-driven cavity with corner heaters. It is observed that the heater length in the x-direction is more effective than that of in the y-direction on the heat transfer and on the flow pattern. The magnetic field affects the average heat transfer rate more on vertical heaters than on the horizontal heaters. Ashorynejad and Shahriari [32] reported numerical results on MHD natural convection of hybrid nanofluid in an open wavy cavity. Öztop *et al.* [33] investigated on mixed convection of MHD flow in a nanofluid filled and partially heated wavy walled lid-driven enclosure. They found that the rate of heat transfer decreases with increasing the Hartmann number. The rate of heat transfer can be enhanced or reduced by increasing the volume fraction of nanoparticles based on Hartmann and Richardson numbers The effect of the location of the

block on mixed convection in a lid-driven cavity with constant heat flux has been reported by Gangawane et al. [34]. Saha et al. [35] investigated the effect of internal heat generation or absorption on MHD mixed convection flow in a lid driven cavity. Pervin and Nasrin [36] studied MHD free convection and heat transfer for different values of Rayleigh numbers Ra and Hartmann numbers Ha in a rectangular enclosure. Their results show that the flow pattern and temperature field are significantly dependent on the used parameters. Chamkha et al. [37] made a study for mixed convection in a square cavity in the presence of magnetic field and an internal heat generation and absorption. He concluded that the flow behavior inside the cavity and heat transfer rate is strongly affected by the magnetic field. Mahmud et al. [38] studied analytically a combined free and forced convection flow of an electrically conducting and heat-generating or absorbing fluid a vertical channel made of two parallel plates under the action of transverse magnetic field. Bakar et. al. [39] has studied the effect of magnetic field on mixed convection heat transfer in a lid-driven square cavity. Basak et al. [40] carried analysis of mixed convection flows within a square cavity with uniform and non-uniform heating of bottom wall. Ali et al. [41] studied the magnetohydrodynamic mixed convection flow in a hexagonal enclosure. They found that Hartmann number and Richardson number have a considerable effect on the flow field and temperature field. Thermally induced convection of molten gallium in magnetic fields is studied by Xu et al. [42]. Manca et al. [43] studied the effect of heated wall position on mixed convection in a channel with an open cavity. They observed that the heat transfer rate decreases with increasing of Hartmann number and heat generation parameter whereas increases for the increasing values of heat absorption parameter. Thus, the magnetic field plays an important role to control heat transfer and fluid flow. The rate of reduction is higher for high values of the Richardson number. Cheong et al. [44] applied various heat sources in a porous shell, including the flow of free convection and internal heat, to explore convection patterns inside a sinusoidal cavity. Chattopadhyay et al. [45] studied mixed convection flow patterns in a dual lid-driven oscillatory heated pore enclosure. That was the top priority of their research to investigate the Darcy impact and even the influence of magnitude and phase variations under sinusoidal boundary conditions, which they accomplished. They saw that the higher magnitude and more significant fluctuations improve heat transmission, and a wavy cavity transfers heat faster than a square cavity. The study related to heat absorption or generation in the confined rectangular enclosures has been well discussed in the literature.

From the above literature review, it is evident that no study has been done on the effect of internal heat generation and absorption in an enclosure having variable undulation in vertical walls. In this study, internal heat generation and absorption on MHD mixed convection heat transfer in an enclosure having variable undulation in vertical walls will be numerically investigated.

## 1.9 PARTICULAR APPLICATIONS

Mixed convection heat transfer has always been of great interest because of its wide range of applications. The relevant research output has numerous applications suchas MHD power generators, radiators in cars, computer CPU heat sinks, hydrogen fuel cells, biological transportation, geophysical fluid mechanics, liquid metal flow control and etc. Magnetic field effects are also important in medicine. Tumors treating fields are said to be a $4^{th}$ treatment in the battle against cancer.

## 1.10 OBJECTIVE OF THE PRESENT STUDY

The aim of proposed research is to investigate the effects of Magneto-Hydrodynamic (MHD) mixed convection flow in a triangular cavity. Results will be presented for different non-dimensional governing and physical parameters in terms of streamlines, isotherms, heat transfer rate as well as the average temperature of the fluid in the cavity.

The specific objectives of the present study are to:

i. Investigate the heat transfer in a lid-driven cavity due to internal heat generation and absorption having wavy side-walls.

ii. Study the effects of physical parameters such as Richardson number, Hartmann number on the flow field for various boundary conditions.

iii. Investigate the effects of applying a variable number of undulations in the vertical walls on the flow field and temperature distribution in terms of streamlines and isotherms.

## 1.11 OUTLINE OF THE THESIS

This dissertation contains five chapters. In chapter 1, a brief introduction is presented together with aim and objectives. This chapter also consists of a literature review of the past studies on fluid flow and heat transfer in cavities. In this state-of-the-art review, different aspects of the previous studies have been mentioned categorically. This is followed by the post-mortem of a recent historical event for the illustration of fluid flow and heat transfer effects in cavities or wavy enclosure.

In Chapter 2, the computational technique of the problem for viscous incompressible flow is discussed in details.

In Chapter 3, mixed convection heat transfer in presence of heat generation or absorption in a lid- driven cavity having variables undulation have been investigated numerically. Mathematical modeling and Finite Element formulation is employed in this study and explained elaborately.

In Chapter 4, a detailed parametric study on mixed convection heat transfer in presence of heat generation or absorption in a lid-driven cavity having variables undulation is conducted. Effects of the major parameters such as Reynolds number, Richardson number, Grashof number and heat generation or absorption on the flow and thermal field with cavity have been presented.

Finally, in Chapter 5 the dissertation is rounded off with the conclusions. Lastly, recommendations for further studies of the present problem are outlined.

## 2.1 INTRODUCTION

The governing equations in fluid dynamics and heat transfer, including conservation forms of the Navier-Stokes system of equations as derived from the first law of thermodynamics, are expressed in terms of the control volume surface integral equations, which represent various physical phenomena. To visualize these thermo-fluid flow scenarios, an approximate numerical solution is needed, which can be obtained by the CFD (Computational Fluid Dynamics) code. The partial differential equations of fluid mechanics and heat transfer are discretized in order to obtain a system of approximate algebraic equations, which then can be solved on a computer. The approximations are applied to small domains in space and time so the numerical solution provides results at discrete locations in space and time. Much as accuracy of experimental data depends on the quality of the tools used, the accuracy of numerical solution is dependent on the quality of discretization used.

CFD computation involves the creation of a set of numbers that constitutes a realistic approximation of a real-life system. The outcome of computation process improves the understanding of the behavior of a system. Thereby, engineers need CFD codes that can produce physically realistic results with good accuracy in simulations with finite grids. Contained within the broad field of computational fluid dynamics are activities that cover the range from the automation of well-established engineering design methods to the use of detailed solutions of the Navier-Stokes equations as substitutes for experimental research into the nature of complex flows. CFD have been used for solving wide range of fluid dynamics problem. It is more frequently used in fields of engineering where the geometry is complicated or some important feature that cannot be dealt with standard methods.

The complete Navier-Stokes equations are considered to be the correct mathematical description of the governing equations of fluid motion. The most accurate numerical computations in fluid dynamics come from solving the Navier-Stokes equations. The equations represent the conservation of mass and momentum. More details are available in Ferziger and Perić [7] and Patankar [6].

## 2.2 ELEMENTS OF A NUMERICAL SOLUTION METHODS

Several elements of numerical solution methods are available in Ferziger and Perić [7], here only the main steps are discussed.

### 2.2.1 Mathematical Model

The primary task of any numerical solution method is to provide a mathematical model, i.e., the set of partial differential equations and its related boundary conditions. A solution method is usually planned for a particular set of equations. Trying to produce a general-purpose solution method, i.e., one which is applicable to all flows, is impractical, is not impossible and as with most general-purpose tools, they are usually not optimum for any one application.

### 2.2.2 Discretization Method

After choosing the mathematical model, one has to select a suitable discretization method, i.e., a method of approximating the differential equations by a system of algebraic equations for the variable at some set of discrete locations in space and time [6].

### 2.2.3 Numerical Grid

The next step is to select a numerical grid that defines the discrete locations, at which the variables are to be calculated. It is essentially a discrete representation of the geometric domain on which the problem is to be solved. It divides the solution domain into a finite number of sub-domains such as elements, control volumes etc. Some of the options available are structural (regular) grid, block structured grid, unstructured grids etc.

### 2.2.4 Element Approximations

Following the choice of grid type, one has to choose the approximations to be used in the discretization process. Approximations for the derivatives at the grid points have to be selected in a finite difference method. In a finite volume method, one has to select the methods of approximating surface and volume integrals. In a finite element method, one has to choose the functions and weighting functions [5].

### 2.2.5 Solution Technique

Discretization yields a large system of non-linear algebraic equations. The method of solution depends on the type of a problem. For unsteady flows, methods based on those used for initial value problems for ordinary differential equation (marching in time) is used. At each time step an elliptic problem has to be solved. Pseudo-time marching or an equivalent iteration scheme usually solves steady flow problems. Since the equations are non-linear, an iteration scheme is

used to solve them. These methods use successive linearization of the equations and the resulting linear systems are almost always solved by iterative techniques. The choice of solver depends on the grid type and the number of nodes involved in each algebraic equation [5].

## 2.3 DISCRETIZATION APPROACHES

One is to consider numerical discretization to solve a mathematical model of physical phenomena. This means that each component of the differential equations is transformed into a "numerical analogue" which can be represented in the computer and then processed by a computer program, built on some algorithm. There are many different methodologies were introduced for this purpose in the past and the development still continues. There are several discretization methods available for the high-performance numerical computation in CFD [6]. These includes but not limited to:

   i.  Finite volume method (FVM)
   ii. Finite element method (FEM)
   iii. Finite difference method (FDM)
   iv. Boundary element method (BEM)
   v.  Boundary volume method (BVM)

In the present numerical computation, Galerkin finite element method (FEM) has been used.

## 2.4 FINITE ELEMENT METHOD

The finite element method (FEM) is a powerful computational technique for solving problems which are described by partial differential equations or can be formulated as functional minimization. The basic idea of the finite element method is to view a given domain as an assemble of simple geometric shapes, called finite elements, for which it is possible to systematically generate the approximation functions needed in the solution of partial differential equations by the variational or weighted residual method. The computational domains with irregular geometries by a collection of finite elements makes the method a valuable practical tool for the solution of boundary, initial and eigen value problems arising in various fields of engineering. The approximation functions, which satisfy the governing equations and boundary conditions, are often constructed using ideas from interpolation theory. Approximating functions in finite elements are determined in terms of nodal values of a physical field which is sought. A continuous physical problem is transformed into a discretized finite element problem with unknown nodal values. For a linear problem, a system of linear

algebraic equations should be solved. Values inside finite elements can be recovered using nodal values. More details are available in Ferziger and Perić [6].

The major steps involved in finite element analysis of a typical problem are:

i.   Discretization of the domain into a set of finite elements (mesh generation).
ii.  Weighted-integral or weak formulation of the differential equation to be analyzed.
iii. Development of the finite element model of the problem using its weighted-integral or weak form.
iv.  Assembly of finite elements to obtain the global system of algebraic equations.
v.   Imposition of boundary conditions.
vi.  Solution of equations.
vii. Post-computation of solution and quantities of interest.

### 2.4.1 Mesh Generation

The first step is to discretize the spatial domain into non-overlapping elements or sub-regions. The Finite Element Method allows a variety of element shapes, for example, triangles, quadrilaterals in two dimensions and tetrahedral, hexahedral, pentahedral, and prisms in three dimensions. Each element is formed by the connection of a certain number of nodes, with the number of nodes in an element depending on the type of the element. The number of nodes in each element does not depend only on the number of corner points in the element, but also on the type of the element interpolation function.
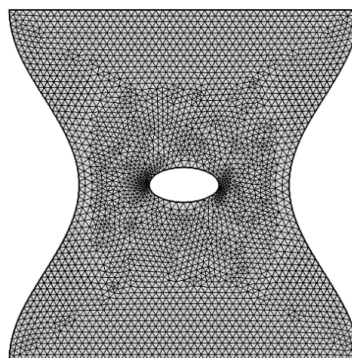


**Figure 2.1:** Current mesh structure of elements of cavity with single undulation

### 2.4.2 Computational Technique

Discretization yields a large system of non-linear algebraic equations. The method of solution depends on the problem. For unsteady flows, methods based on those used for initial value problems for ordinary differential equation (marching in time) isused. At each time step an elliptic problem has to be solved. Pseudo-time marchingor an equivalent iteration scheme

21

usually solves steady flow problems. Since the equations are non-linear, an iteration scheme is used to solve them. These methods use successive linearization of the equations and the resulting linear systems are almost always solved by iterative techniques. The choice of solver depends on the grid type and the number of nodes involved in each algebraic equation.

## 2.5 ALGORITHM
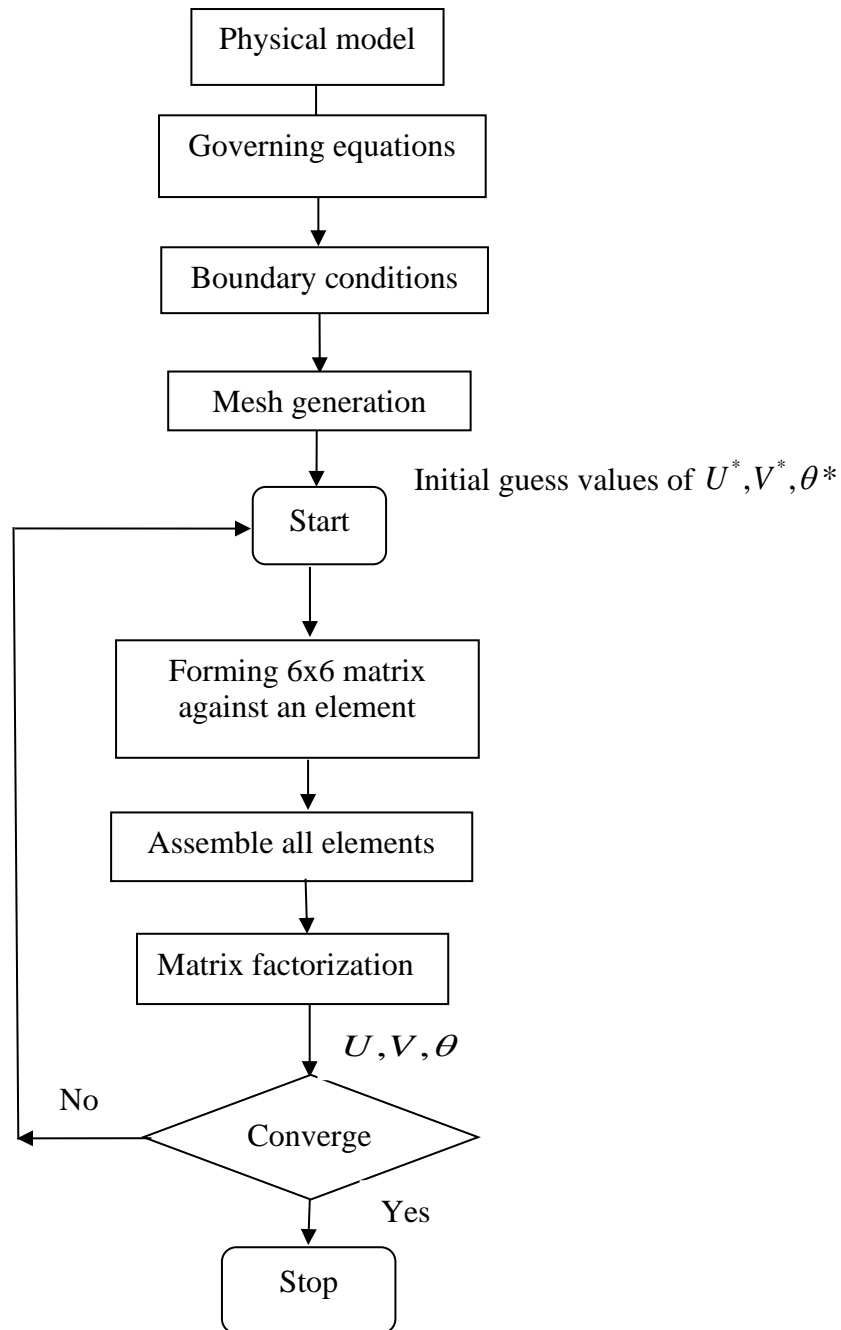


**Figure 2.2:** Flow chart of the computational procedure

The algorithm was originally put forward by the iterative Newton-Raphson algorithm; the discrete forms of the continuity, momentum and energy equations are solved to find out the

value of the velocity and the temperature. It is essential to guess the initial values of the variables. Then the numerical solutions of the variables are obtained while the convergent criterion is fulfilled. The simple algorithm is shown by the flow chart below.

### 2.5.1 Solution of System of Equations

A system of linear algebraic equations is solved by the UMFPACK with MATLAB interface. UMFPACK is a set of routines for solving asymmetric sparse linear systems Ax = b, using the Asymmetric Multifrontal method and direct sparse LU factorization. Following primary UMFPACK routines are required to factorize A or Ax = b:

  i. Pre-orders the columns of A to reduce fill-in and performs a symbolic analysis.
  ii. Numerically scales and then factorizes a sparse matrix.
  iii. Solves a sparse linear system using the numeric factorization.
  iv. Frees the symbolic object.
  v. Frees the numeric object.

Additional routines are:

  i.  Passing a different column ordering
  ii. Changing default parameters
  iii. Manipulating sparse matrices
  iv. Getting LU factors
  v. Solving the LU factors
  vi. Computing determinant

UMFPACK factorizes PAQ, PRAQ, or $PR^{-1}AQ$ into the product LU, where L and U are lower and upper triangular matrices respectively, P and Q are permutation matrices, and R is a diagonal matrix of row scaling factors (or R = I if row-scaling is not used). Both P and Q are chosen to reduce fill-in (new non-zeros in L and U that are not present in A). The permutation P has the dual role of reducing fill-in and maintaining numerical accuracy (via relaxed partial pivoting and row interchanges). The sparse matrix A can be square or rectangular, singular or non-singular, and real or complex (or any combination). Only square matrices A can be used to solve $Ax = b$ or related systems. Rectangular matrices can only be factorized. UMFPACK first finds a column pre-ordering that reduces fill-in, without regard to numerical values. It scales and analyzes the matrix, and then automatically selects one of three strategies for pre-ordering the rows and columns: asymmetric, 2-by-2 and symmetric. These strategies are described below.

One notable attribute of the UMFPACK is that whenever a matrix is factored, the factorization is stored as a part of the original matrix so that further operations on the matrix can reuse this factorization. Whenever a factorization or decomposition is calculated, it is preserved as a list (element) in the factor slot of the original object. In this way a sequence of operations, such as determining the condition number of a matrix and then solving a linear system based on the matrix, do not require multiple factorizations of the intermediate results.

Conceptually, the simplest representation of a sparse matrix is as a triplet of an integer vector $i$ giving the row numbers, an integer vector $j$ giving the column numbers, and a numeric vector $x$ giving the non-zero values in the matrix. The triplet representation is row-oriented if elements in the same row were adjacent and column-oriented if elements in the same column were adjacent. The compressed sparse row or compressed sparse column representation is similar to row-oriented triplet or column-oriented triplet respectively. These compressed representations remove the redundant row or column in indices and provide faster access to a given location in the matrix.

## 3.1 ITRODUCTION

Mathematical model of physical phenomena may be ordinary or partial differential equations, which have been the subject of analytical and numerical investigations. The partial differential equations of fluid mechanics and heat transfer are solvable for only a limited number of flows. To obtain an approximate solution numerically, we have to use a discretization method, which approximated the differential equations by a system of algebraic equations, which can then be solved on a computer. The approximations are applied to small domains in space and time so the numerical solution provides results at discrete locations in space and time.

## 3.2 PHYSICAL MODEL

A two-dimensional cavity with heat absorption and generation source is considered for the present study with the physical dimension as shown in Fig. 3.1. The upper wall of the cavity is allowed to move from left to right to its own plane at a constant speed $U_0$ and the other walls have no-slip condition. The cavity bottom wall is maintained at a high temperature $T_h$, to induce buoyancy effect and the upper wall is insulated. The two vertical walls are maintained at cold temperature $T_c$, $T_h > T_c$. The gravitational force acts in the vertically downward direction and uniform magnetic field with a constant magnitude $(B_0)$ in the opposite direction of the moving lid is applied.
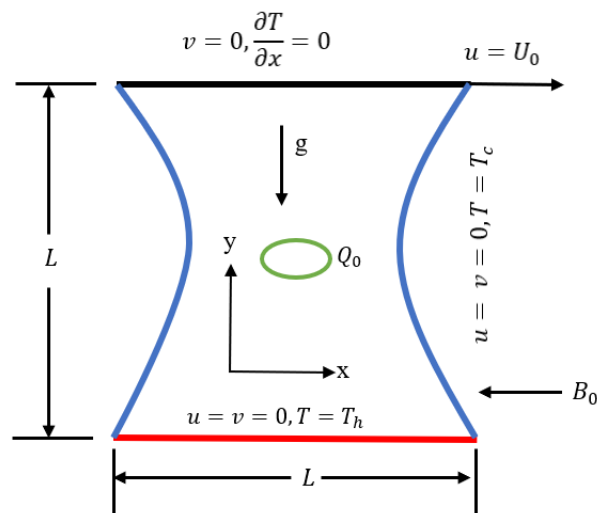


**Figure 3.1:** Schematic diagram of the cavity with boundary conditions

## 3.3 GOVERNING EQUATIONS ALONG WITH BOUNDARY CONDITIONS

The electrically conducting fluids are assumed to be Newtonian fluids with constant fluid properties, except for the density in the buoyancy force term. Moreover, the fluid is considered to be laminar, incompressible, steady and two-dimensional. It is assumed that the induced magnetic field produced by the motion of an electrically conducting fluid is negligible compared to the applied magnetic field. This assumption uncouples the Navier-Stokes equations from Maxwell's equations. No electric field is present and the hall effect is neglected. The thermo-physical properties of the fluid are assumed to be constant, except the density variation in the buoyancy term which is treated according to Boussinesq approximation while viscous dissipation effects are considered negligible.

With above mentioned assumptions, the governing equations for conservations of mass, momentum and energy proposed by Saha et al. [35] can be written as

Mass conservation equation:

$$\frac{\partial u}{\partial x} + \frac{\partial v}{\partial y} = 0 \tag{3.1}$$

Momentum conservation equation:

$$u\frac{\partial u}{\partial x} + v\frac{\partial u}{\partial y} = -\frac{1}{\rho}\frac{\partial p}{\partial x} + \vartheta\left(\frac{\partial^2 u}{\partial x^2} + \frac{\partial^2 u}{\partial y^2}\right) \tag{3.2}$$

$$u\frac{\partial v}{\partial x} + v\frac{\partial v}{\partial y} = -\frac{1}{\rho}\frac{\partial p}{\partial y} + \vartheta\left(\frac{\partial^2 v}{\partial x^2} + \frac{\partial^2 v}{\partial y^2}\right) + g\beta(T - T_c) - \frac{\sigma B_0^2 v}{\rho} \tag{3.3}$$

Energy conservation equation:

$$u\frac{\partial T}{\partial x} + v\frac{\partial T}{\partial y} = \alpha\left(\frac{\partial^2 T}{\partial x^2} + \frac{\partial^2 T}{\partial y^2}\right) + \frac{Q_0}{\rho c_p}(T - T_c) \tag{3.4}$$

where $x$ and $y$ are the distances measured along the horizontal and vertical directions respectively; $u$ and $v$ are the velocity components in the $x$ and $y$ directions respectively; $T$ denote the fluid temperature, $T_c$ denotes the cold temperature, $p$ is the pressure and $\rho$ is the fluid density, $g$ is the gravitational constant, $\beta$ is the volumetric coefficient of thermal expansion, $c_p$ is the specific heat at constant pressure, $\kappa$ is the thermal conductivity of fluid. The parameters $\alpha, \beta_0$ and $Q_0$ are the thermal diffusivity of the fluid, magnetic induction, and the volumetric internal heat generation $Q_0 > 0$, or absorption $Q_0 < 0$ coefficient respectively.

### 3.3.1 Boundary Conditions

The boundary conditions for the present problem are specified as follows:

On the top walls: $u = U_0, v = 0, \dfrac{\partial T}{\partial x} = 0$ *for* $0 \le x \le 1, y = 1$.

On the bottom walls: $u = v = 0, T = T_h$ *for* $0 \le x \le 1, y = 0$.

On left vertical wavy wall: $u = v = 0, T = T_c$, *for* $x = A(1 - \cos(2\pi\lambda y)), 0 \le y \le 1$.

On right vertical wavy wall: $u = v = 0, T = T_c$, *for* $x = 1 - A(1 - \cos(2\pi\lambda y)), 0 \le y \le 1$.

where $A$ is the amplitude and $\lambda$ are the number of undulations.

Solid fluid interface boundary conditions:

$$u = v = 0$$

$$T_f = T_s$$

$$\kappa_f \cdot \left(\frac{\partial T}{\partial n}\right)_f = \kappa_s \cdot \left(\frac{\partial T}{\partial n}\right)_s,$$

Where

$T_f$ = temperature for fluid

$T_s$ = temperature for solid

$\kappa_f$ = thermal conductivity for fluid

$\kappa_s$ = thermal conductivity for solid

$\left(\frac{\partial T}{\partial n}\right)_f$ = temperature gradient for fluid

$\left(\frac{\partial T}{\partial n}\right)_s$ = temperature gradient for solid

$n$ = the normal direction vector of the surface

### 3.3.2 Dimensional Analysis

Non-dimensional variables are used for transforming the governing equations $(3.1 - 3.4)$ into dimensionless form. These are stated as follows:

$$X = \frac{x}{L}, Y = \frac{y}{L}, U = \frac{u}{U_0}, V = \frac{v}{U_0}, P = \frac{p}{\rho U_0{}^2}, \theta = \frac{(T - T_c)}{(T_h - T_c)},$$

where $X$ and $Y$ are the coordinates varying along horizontal and vertical directions, respectively, $U$ and $V$ are the velocity components in the $X$ and $Y$ directions, respectively, $\theta$ is the dimensionless temperature and $P$ is the dimensionless pressure. After substitution the dimensionless variables into the equations $(3.1 - 3.4)$, we get the following dimensionless equations:

Mass conservation equation:

$$\frac{\partial U}{\partial X} + \frac{\partial V}{\partial Y} = 0 \qquad\qquad (3.5)$$

Momentum conservation equation:

$$U\frac{\partial U}{\partial X} + V\frac{\partial U}{\partial Y} = -\frac{\partial P}{\partial X} + \frac{1}{Re}\left(\frac{\partial^2 U}{\partial X^2} + \frac{\partial^2 U}{\partial Y^2}\right) \qquad\qquad (3.6)$$

$$U\frac{\partial V}{\partial X} + V\frac{\partial V}{\partial Y} = -\frac{\partial P}{\partial Y} + \frac{1}{Re}\left(\frac{\partial^2 V}{\partial X^2} + \frac{\partial^2 V}{\partial Y^2}\right) + Ri\,\theta - \frac{Ha^2}{Re}V \qquad\qquad (3.7)$$

Energy conservation equation:

$$U\frac{\partial \theta}{\partial X} + V\frac{\partial \theta}{\partial Y} = \frac{1}{Re\,Pr}\left(\frac{\partial^2 \theta}{\partial X^2} + \frac{\partial^2 \theta}{\partial Y^2}\right) + \frac{\Delta\theta}{Re\,Pr}, \qquad\qquad (3.8)$$

The dimensionless parameters appearing in the equations (2.6) through (2.8) are the Grashof number ($Gr$), Reynolds number($Re$), Prandtl number ($Pr$), Richardson number ($Ri$), and Hartmann number ($Ha$). They are respectively defined as follows:

$$Re = \frac{U_0 L}{\nu},\, Pr = \frac{\nu}{\alpha},\, Ha^2 = \frac{\sigma B_0^2 L^2}{\mu},\, Gr = \frac{g\beta\Delta T L^3}{\nu^2}\, and\, Ri = \frac{Gr}{Re^2} = \frac{UL}{\nu},$$

where $\Delta = \dfrac{Q_0 L^2}{\alpha\rho c_p}$ is the heat generation or absorption co-efficient.

### 3.3.3 Boundary Conditions (non-dimensional)

The dimensionless boundary conditions under consideration can be written as:

On the top walls: $U = 1, V = 0, \dfrac{\partial \theta}{\partial X} = 0\ for\, 0 \le X \le 1, Y = 1.$

On the bottom walls: $U = 0, V = 0, \theta = 1\ for\, 0 \le X \le 1, Y = 0.$

On left vertical wavy wall: $U = V = 0, \theta = 0,\, for\, X = A(1 - \cos(2\pi\lambda Y)), 0 \le Y \le 1.$

On right vertical wavy wall: $U = V = 0, \theta = 0,\, for\, X = 1 - A(1 - \cos(2\pi\lambda Y)), 0 \le Y \le 1.$

Solid fluid interface boundary conditions: $U = V = 0$

$$\theta_f = \theta_s$$

$$\left(\frac{\partial \theta}{\partial N}\right)_f = k.\left(\frac{\partial \theta}{\partial N}\right)_s,$$

Where

$$k = \frac{k_s}{k_f}.$$

### 3.3.4 Nusselt Number

The heat transfer by conduction was equated to the heat transfer by convection

$$h \times \Delta T = -k \frac{\partial T}{\partial n} \tag{3.9}$$

where $n$ is the non-dimensional distances either along x or y-direction acting normal to the surface. By introducing the dimensionless variables into equation (3.9) the local Nusselt number is defined as:

$$Nu_L = -\left. \frac{\partial \theta}{\partial n} \right|_{wall} \tag{3.10}$$

According to Singh and Sharif (2003), the average Nusselt number at the heated wall of the cavity based on the no-dimensional variables may be expressed as

$$Nu_{av} = -\int_0^1 \left. \frac{\partial \theta}{\partial n} \right|_{wall} \tag{3.11}$$

### 3.4 NUMERICAL ANALYSIS

The governing equations along with the boundary conditions are solved numerically, employing Galerkin weighted residual finite element techniques as discussed below.

### 3.4.1 Finite Element Formulation and Computational Procedure

To derive the finite element equations, the method of weighted residuals due to Zienkiewicz and Taylor [29] is applied to the equations (3.5) – (3.8) as

$$\int_A N_\alpha \left( \frac{\partial U}{\partial X} + \frac{\partial V}{\partial Y} \right) dA = 0 \tag{3.12}$$

$$\int_A N_\alpha \left( U \frac{\partial U}{\partial X} + V \frac{\partial U}{\partial Y} \right) dA = -\int_A H_\lambda \left( \frac{\partial P}{\partial X} \right) dA + \frac{1}{Re} \int_A N_\alpha \left( \frac{\partial^2 U}{\partial X^2} + \frac{\partial^2 U}{\partial Y^2} \right) dA \tag{3.13}$$

$$\int_A N_\alpha \left( U \frac{\partial V}{\partial X} + V \frac{\partial V}{\partial Y} \right) dA = -\int_A H_\lambda \left( \frac{\partial P}{\partial Y} \right) dA + \frac{1}{Re} \int_A N_\alpha \left( \frac{\partial^2 V}{\partial X^2} + \frac{\partial^2 V}{\partial Y^2} \right) dA$$

$$+ Ri \int_A N_\alpha \theta \, dA - \frac{Ha^2}{Re} \int_A N_\alpha V \, dA \tag{3.14}$$

$$\int_A N_\alpha \left( U \frac{\partial \theta}{\partial X} + V \frac{\partial \theta}{\partial Y} \right) dA = \frac{1}{Re\,Pr} \int_A N_\alpha \left( \frac{\partial^2 \theta}{\partial X^2} + \frac{\partial^2 \theta}{\partial Y^2} \right) dA + \frac{\Delta}{Re\,Pr} \int N_\alpha \theta dA \tag{3.15}$$

where $A$ is the element area, $N_\alpha$ ( $\alpha = 1, 2, \ldots \ldots, 6$) are the element interpolation functions for the velocity components and the temperature, and $H_\lambda$ ( $\lambda = 1, 2, 3$) are the element interpolation functions for the pressure.

Gauss's theorem is then applied to equations (3.13) -(3.15) to generate the boundary integral terms associated with the surface tractions and heat flux. Then equations (3.13) -(3.15) become,

$$\int_A N_\alpha \left( U \frac{\partial U}{\partial X} + V \frac{\partial U}{\partial Y} \right) dA + \int_A H_\lambda \left( \frac{\partial P}{\partial X} \right) dA$$
$$- \frac{1}{Re} \int_A \left( \frac{\partial N_\alpha}{\partial X} \frac{\partial U}{\partial X} + \frac{\partial N_\alpha}{\partial Y} \frac{\partial U}{\partial Y} \right) dA = \int_{S_0} N_\alpha S_x dS_0 \tag{3.16}$$

$$\int_A N_\alpha \left( U \frac{\partial V}{\partial X} + V \frac{\partial V}{\partial Y} \right) dA + \int_A H_\lambda \left( \frac{\partial P}{\partial Y} \right) dA - \frac{1}{Re} \int_A \left( \frac{\partial N_\alpha}{\partial X} \frac{\partial V}{\partial X} + \frac{\partial N_\alpha}{\partial Y} \frac{\partial V}{\partial Y} \right) dA$$
$$- Ri \int_A N_\alpha \, \theta \, dA + \frac{Ha^2}{Re} \int_A N_\alpha V \, dA = \int_{S_0} N_\alpha S_y dS_0 \tag{3.17}$$

$$\int_A N_\alpha \left( U \frac{\partial \theta}{\partial X} + V \frac{\partial \theta}{\partial Y} \right) dA - \frac{1}{Re\,Pr} \int_A \left( \frac{\partial N_\alpha}{\partial X} \frac{\partial \theta}{\partial X} + \frac{\partial N_\alpha}{\partial Y} \frac{\partial \theta}{\partial Y} \right) dA -$$

$$\frac{\Delta}{Re\,Pr} \int_A N_\alpha \theta \, dA = \int_{S_w} N_\alpha \, q_w \, dS_w \tag{3.18}$$

Here (3.16) -(3.17) specifying surface tractions $(S_x, S_y)$ along outflow boundary $S_0$ and (3.18) specifying velocity components and fluid temperature or heat flux $(q_w)$ that flows into or out from domain along wall boundary $S_w$.

The basic unknowns for the above differential equations are the velocity components $U, V$ the temperature, $\theta$ and the pressure, $P$. The six-node triangular element is used in this work for the development of the finite element equations. All six nodes are associated with velocities as well as temperature; only the corner nodes are associated with pressure. This means that a lower order polynomial is chosen for pressure and which is satisfied through continuity equation. The velocity component and the temperature distributions and linear interpolation for the pressure distribution according to their highest derivative orders in the differential equations (3.5) -(3.8) as

$$U(X, Y) = N_\beta U_\beta \tag{3.19}$$

$$V(X,Y) = N_\beta V_\beta \tag{3.20}$$

$$\theta(X,Y) = N_\beta \theta_\beta \tag{3.21}$$

$$P(X,Y) = H_\lambda P_\lambda \tag{3.22}$$

where $\beta = 1, 2, \ldots \ldots, 6; \lambda = 1, 2, 3.$

Substituting the element velocity component distributions, the temperature distribution, and the pressure distribution from equations (3.19) - (3.22), we get the following equations

$$\int_A N_\alpha (N_{\beta,x} U_\beta + N_{\beta,y} V_\beta) = 0 \tag{3.23}$$

$$\int_A N_\alpha [(N_\beta U_\beta)(N_{\gamma,x} U_\gamma) + (N_\beta V_\beta)(N_{\gamma,y} U_\gamma)] dA + \int_A H_\lambda H_{\mu,x} P_\mu dA -$$
$$\frac{1}{Re} \int_A (N_{\alpha,x} N_{\beta,x} U_\beta + N_{\alpha,y} N_{\beta,y} U_\beta) dA = \int_{S_0} N_\alpha S_x dS_0 \tag{3.24}$$

$$\int_A N_\alpha [(N_\beta U_\beta)(N_{\gamma,x} V_\gamma) + (N_\beta V_\beta)(N_{\gamma,y} V_\gamma)] dA + \int_A H_\gamma H_{\mu,y} P_\mu dA -$$
$$\frac{1}{Re} \int_A (N_{\alpha,x} N_{\beta,x} V_\beta + N_{\alpha,y} N_{\beta,y} V_\beta) dA - Ri \int_A N_\alpha N_\beta \theta_\beta dA +$$
$$\frac{Ha^2}{Re} \int_A N_\alpha N_\beta V_\beta dA = \int_{S_0} N_\alpha S_y dS_0 \tag{3.25}$$

$$\int_A N_\alpha [(N_\beta U_\beta)(N_{\gamma,x} \theta_\gamma) + (N_\beta V_\beta)(N_{\gamma,y} \theta_\gamma)] dA -$$
$$\frac{1}{RePr} \int_A (N_{\alpha,x} N_{\beta,x} \theta_\beta + N_{\alpha,y} N_{\beta,y} \theta_\beta) dA - \frac{\Delta}{PrRe} \int_A N_\alpha N_\beta \theta_\beta dA$$
$$= \int_{S_w} N_\alpha q_w dS_w \tag{3.26}$$

Then the finite element equations can be written in the form,

$$K_{\alpha\beta^x} U_\beta + K_{\alpha\beta^y} V_\beta = 0 \tag{3.27}$$

$$K_{\alpha\beta\gamma^x} U_\beta U_\gamma + K_{\alpha\beta\gamma^y} V_\gamma U_\gamma + M_{\alpha\mu^x} P_\mu - \frac{1}{Re}\left(S_{\alpha\beta^{xx}} + S_{\alpha\beta^{yy}}\right) U_\beta = Q_{\alpha^u} \tag{3.28}$$

$$K_{\alpha\beta\gamma^x} U_\beta V_\gamma + K_{\alpha\beta\gamma^y} V_\beta V_\gamma + M_{\alpha\mu^y} P_\mu - \frac{1}{Re}\left(S_{\alpha\beta^{xx}} + S_{\alpha\beta^{yy}}\right) V_\beta$$
$$-\frac{Gr}{Re^2} K_{\alpha\beta} \theta_\beta + \frac{Ha^2}{Re} K_{\alpha\beta} V_\beta = Q_{\alpha^v} \tag{3.29}$$

$$K_{\alpha\beta\gamma^x} U_\beta \theta_\gamma + K_{\alpha\beta\gamma^y} V_\beta \theta_\gamma - \frac{1}{RePr}\left(S_{\alpha\beta^{xx}} + S_{\alpha\beta^{yy}}\right) \theta_\beta - \frac{\Delta}{RePr} K_{\alpha\beta} \theta_\beta = Q_{\alpha^\theta} \tag{3.30}$$

where the coefficients in element matrices are in the form of the integrals over the element area and along the element edges $S_0$ and $S_w$ as

$$K_{\alpha\beta^x} = \int_A N_\alpha N_{\beta,x} dA \tag{3.31a}$$

31

$$K_{\alpha\beta,y} = \int_A N_\alpha N_{\beta,y} dA \tag{3.31b}$$

$$K_{\alpha\beta\gamma^x} = \int_A N_\alpha N_\beta N_{\gamma,x} dA \tag{3.31c}$$

$$K_{\alpha\beta\gamma^y} = \int_A N_\alpha N_\beta N_{\gamma,y} dA \tag{3.31d}$$

$$K_{\alpha\beta} = \int_A N_\alpha N_\beta dA \tag{3.31e}$$

$$S_{\alpha\beta^{xx}} = \int_A N_{\alpha,x} N_{\beta,x} dA \tag{3.31f}$$

$$S_{\alpha\beta^{yy}} = \int_A N_{\alpha,y} N_{\beta,y} dA \tag{3.31g}$$

$$M_{\alpha\mu^x} = \int_A H_\alpha H_{\mu,x} dA \tag{3.31h}$$

$$M_{\alpha\mu^y} = \int_A H_\alpha H_{\mu,y} dA \tag{3.31i}$$

$$Q_{\alpha^u} = \int_{S_0} N_\alpha S_x dS_0 \tag{3.31j}$$

$$Q_{\alpha^v} = \int_{S_0} N_\alpha S_y dS_0 \tag{3.31k}$$

$$Q_{\alpha\theta} = \int_{S_w} N_\alpha q_w dS_w \tag{3.31\textit{l}}$$

These element matrices are evaluated in closed form ready for numerical simulation. Details of the derivation for these element matrices are omitted here in.

The derived finite element equations (3.27) -(3.30) are nonlinear. These nonlinear algebraic equations are solved by applying the Newton-Raphson iteration technique by first writing the unbalanced values from the set of the finite element equations (3.27) -(3.30) as

$$F_{\alpha^p} = K_{\alpha\beta^x} U_\beta + K_{\alpha\beta^y} V_\beta \tag{3.32a}$$

$$F_{\alpha^u} = K_{\alpha\beta\gamma^x} U_\beta U_\gamma + K_{\alpha\beta\gamma^y} V_\gamma U_\gamma + M_{\alpha\mu^x} P_\mu$$
$$- \frac{1}{Re}(S_{\alpha\beta^{xx}} + S_{\alpha\beta^{yy}})U_\beta - Q_{\alpha^u} \tag{3.32b}$$

$$F_{\alpha^v} = K_{\alpha\beta\gamma^x} U_\beta V_\gamma + K_{\alpha\beta\gamma^y} V_\gamma V_\gamma + M_{\alpha\mu^y} P_\mu -$$
$$\frac{1}{Re}(S_{\alpha\beta^{xx}} + S_{\alpha\beta^{yy}})V_\beta - Ri\, K_{\alpha\beta}\theta_\beta + \frac{Ha^2}{Re} K_{\alpha\beta} V_\beta - Q_{\alpha^v} \tag{3.32c}$$

$$F_{\alpha\theta} = K_{\alpha\beta\gamma^x}U_\beta\theta_\gamma + K_{\alpha\beta\gamma^y}V_\beta\theta_\gamma - \frac{1}{Re\,Pr}\left(S_{\alpha\beta^{xx}} + S_{\alpha\beta^{yy}}\right)\theta_\beta$$

$$-\frac{\Delta}{Re\,Pr}K_{\alpha\beta}\theta_\beta - Q_{\alpha\theta} \tag{3.32d}$$

This leads to a set of algebraic equations with the incremental unknowns of the element nodal velocity components, temperatures, and pressures in the form

$$\begin{bmatrix} K_{uu} & K_{uv} & K_{u\theta} & K_{up} \\ K_{vu} & K_{vv} & K_{v\theta} & K_{vp} \\ K_{\theta u} & K_{\theta v} & K_{\theta\theta} & 0 \\ K_{pu} & K_{pv} & 0 & 0 \end{bmatrix} \begin{bmatrix} \Delta u \\ \Delta v \\ \Delta\theta \\ \Delta p \end{bmatrix} = \begin{bmatrix} F_{\alpha^u} \\ F_{\alpha^v} \\ F_{\alpha^\theta} \\ F_{\alpha^p} \end{bmatrix} \tag{3.33}$$

*Where,*

$$K_{uu} = K_{\alpha\beta\gamma^x}U_\beta + K_{\alpha\beta\gamma^x}U_\gamma + K_{\alpha\beta\gamma^x}V_\beta - \frac{1}{Re}\left(S_{\alpha\beta^{xx}} + S_{\alpha\beta^{yy}}\right)$$

$$K_{uv} = K_{\alpha\beta\gamma^y}U_\gamma$$

$$K_{u\theta} = 0$$

$$K_{up} = M_{\alpha\mu^x}$$

$$K_{vu} = K_{\alpha\beta\gamma^x}V_\gamma$$

$$K_{vv} = K_{\alpha\beta\gamma^x}U_\beta + K_{\alpha\beta\gamma^y}V_\gamma + K_{\alpha\beta\gamma^y}V_\gamma - \frac{1}{Re}\left(S_{\alpha\beta^{xx}} + S_{\alpha\beta^{yy}}\right) + \frac{Ha^2}{Re}K_{\alpha\beta}$$

$$K_{v\theta} = -RiK_{\alpha\beta}$$

$$K_{vp} = M_{\alpha\mu^y}$$

$$K_{\theta u} = K_{\alpha\beta\gamma^x}\theta_\gamma$$

$$K_{\theta v} = K_{\alpha\beta\gamma^y}\theta_\gamma$$

$$K_{\theta\theta} = K_{\alpha\beta\gamma^x}U_\beta + K_{\alpha\beta\gamma^y}V_\beta - \frac{1}{Re\,Pr}\left(S_{\alpha\beta^{xx}} + S_{\alpha\beta^{yy}}\right) - \frac{\Delta}{Re\,Pr}K_{\alpha\beta}$$

$$K_{pu} = M_{\alpha\mu^x}$$

$$K_{pv} = M_{\alpha\mu^y} \text{ and } K_{\theta p} = K_{p\theta} = K_{pp} = 0$$

The iteration process is terminated if the percentage of the overall change compared to the previous iteration is less than the specified value of the error estimation of convergence criterion.

To solve the sets of the global nonlinear algebraic equations in the form of matrix, the Newton-Raphson iteration technique has been adapted through PDE solver. The convergence of solutions is assumed when the relative error for each variable between consecutive iterations

is recorded below the convergence criterion ε such that $|\Psi^{n+1} - \Psi^n| < \varepsilon$, where n is number of iteration and $\Psi = U, V, \theta$. The convergence criterion was set to $\varepsilon = 10^{-5}$.

### 3.4.2 Grid Size Sensitivity Test

In order to determine a proper grid size for the present study at $Pr = 0.70, \lambda = 2, Ha = 20, Re = 10^2, Gr = 10^4$ and $\Delta = 6$, A grid independent test was analyzed with five types of meshes, average Nusselt number on the bottom heated wall is obtained. This is described in Table 3.1 and as seen in Figure 3.2.

**Table 3.1:** Grid sensitivity check at $Pr = 0.70, \lambda = 2, Ha = 20, Re = 10^2, Gr = 10^4$ and $\Delta = 6$.

| Nodes | 433 | 816 | 1309 | 3206 | 11722 |
|---|---|---|---|---|---|
| Elements | 762 | 1484 | 2432 | 6136 | 22920 |
| $Nu_{av}$ | 6.941 | 7.560 | 7.839 | 7.954 | 7.995 |

Table 3.1 and figure in the bottom row is presenting the average Nusselt number on the bottom heated wall for different grids. As it can be observed from the table, the grid size of 3206 nodes and 6136 elements provided a satisfactory solution for the present numerical investigation.
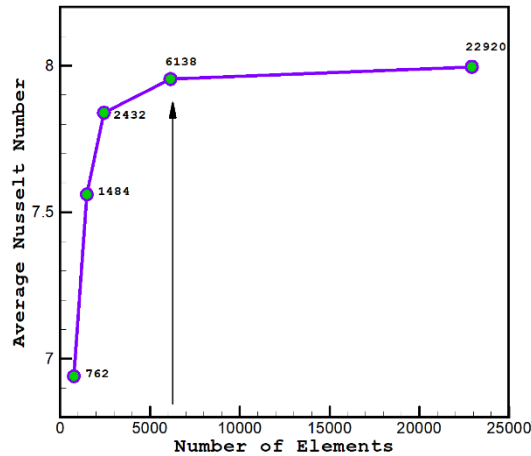


**Figure 3.2:** Grid independency study for different elements while $Pr = 0.70, \lambda = 2, Ha = 20, Re = 10^2, Gr = 10^4$ and $\Delta = 6$.

### 3.4.3 Validation of the Numerical Scheme

In order to check the accuracy of the numerical results obtained throughout the present study is verified against numerical studies reported by Basak et al. [40]. In absence of the magnetic (Ha = 0) and heat generation or absorption ($\Delta = 0$) effects present model is consistent with those of Basak et al. [40]. The comparison for the contour maps of

temperature is presented in Figures 3.2 for $Re = 1$ and $Gr = 10^3, 10^4$ and $10^5$. It is clear that excellent agreement between the present numerical solutions and those of Basak et al. [40] exists.
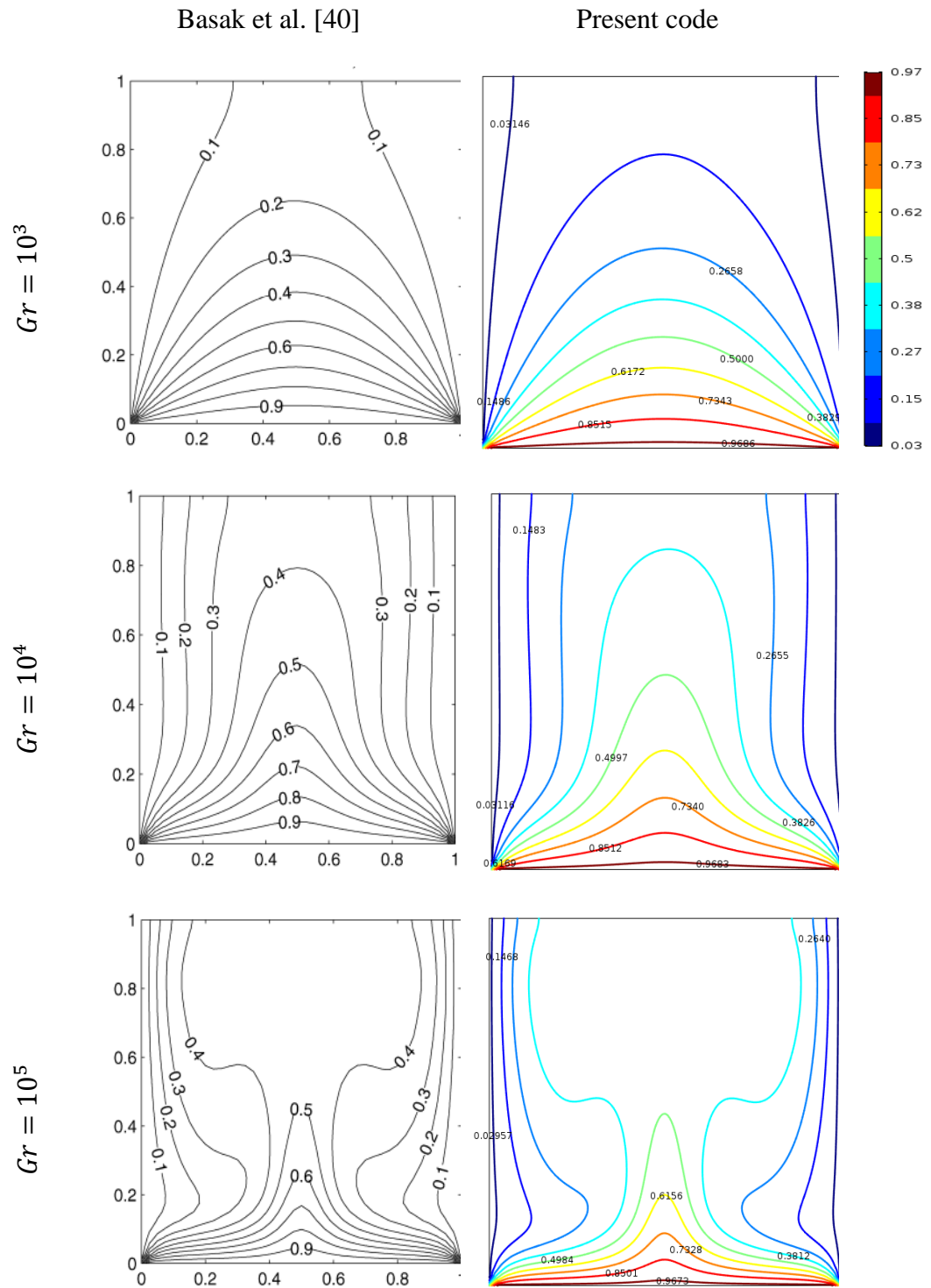


**Figure 3.3:** Comparison of isotherm contour obtained from present code and Basak et al. [40]. for $Pr = 0.70, Ha = 10 \; and \; Re = 1$.

## 4.1 INTRODUCTION

A numerical study has been performed through the finite element method to analyze the effects of internal heat generation or absorption on laminar mixed convection heat transfer and fluid flow in a lid-driven cavity having variable undulation. Numerical results are presented in order to determine the effects of the considered parameters. The internal heat generation or absorption($\Delta$), dimensionless parameters specified for the system are Reynold's number ($Re$), Richardson number ($Ri$) Grashof number ($Gr$) and physical parameter for the number of undulation ($\lambda$) of the cavity. Results are presented through streamline and isotherms along with necessary plots at the four different internal temperature $\Delta = -6, -3, 3$ and $6$ along with different undulation $\lambda = 1, 2, 3$, amplitude $A = 0.1$, Hartman Number $Ha = 20$ and Prandtl number $Pr = 0.70$ for different values of $Re = 1$ to $2000$, $Gr = 1$ to $10^6$ and $Ri = 0.1$ to $10$. Furthermore, the velocity profiles and heat transfer rate in terms of the average Nusselt number $Nu_{av}$ and the average fluid temperature $\theta_{av}$ are displayed.

## 4.2 EFFECT OF REYNOLDS NUMBER

In this section, results of the numerical investigation of the effect of Reynold's Number on MHD mixed convection heattransfer in presence of heat generation or absorption in a lid-driven cavity having one undulation are numerically presented. The results have been obtained for the Reynold' number $Re = 100, 500, 1000$ and $2000$ as shown in Figure 4.1- 4.6.

### 4.2.1 Effect of Reynolds Number for Heat Absorption ($\Delta = -6$)

The effects of Reynold number $Re$ ($= 100, 500, 1000$ & $2000$) on streamlines and isotherms for the present configuration at $Ha = 20, Pr = 0.70, A = 0.1, \Delta = -6$ and $\lambda = 1$ has been demonstrated in Figure 4.1(a)–(b). Reynold's number represents the relative importance of mixed convection. From Figure 4.1 (a), it is seen that when $Re = 100$ the strength of buoyancy force inside the cavity is significant and two vortices appear inside thecavity which one is major vortex and another one is minor vortex.Again, when $Re = 500$ the flow structure is similar to $Re = 100$ but secondary vortices disappear inside the cavity. Further again when Reynold's number increases ($Re = 1000$ and $2000$), the strength of the buoyancy force is more significant and two vortices appear inside the enclosure. For $Re = 1000$ the secondary vortex appears to right cold wall and the cells distance is minimum.

**Figure 4.1:** Effect of Reynolds number on (a) streamlines and (b) isotherms for $Pr = 0.70, \lambda = 1, Ha = 20, Gr = 10^4 \ and \ \Delta = -6$.

Again, for $Re = 2000$ the secondary vortex appears to the left cold wall and the cells distance of primary vortex is also decreased. The physical fact behind it is that the greater effect of the Reynold's number increases the buoyancy force to influence the flow field.

On the other hand, in Figure 4.1(b), isotherms are distributed near the bottom wall as it was isothermally heated. Moreover, it occupies the half of the cavity and some isotherms are also concentrated with the centered ellipse as it was heat absorbed. For $Re = 100, 500, 1000$ the vertical heat gradient takes part near the left wall but in case of $Re = 2000$ near the right wall. In addition, the isotherms are effectively close toward the hot wall as $Re$ is increased. At each increment in $Re$ numbers, there is a clear change in isotherms distribution compared to previous one.

**4.2.2 Effect of Reynolds Number for Heat Absorption ($\Delta = -3$)**

The effects of Reynold's number $Re (= 100, 500, 1000, 2000)$on streamlines and isotherms for the present configuration at $Ha = 20, Pr = 0.70, A = 0.1, \Delta = -3 \ and \ \lambda = 1$ has been demonstrated in Figure 4.2-(a)–(b). From Figure 4.2 (a), it is seen that the strength of buoyancy force inside the cavity is almost similar as in the case heat absorption $\Delta = -6$. But cell distance is less compared to the case $\Delta = -6$. Which implies that the flow strength and velocity increased with decreased of heat absorption. On the other hand, in Figure 4.2(b), isotherms are distributed near the bottom wall as it was isothermally heated. Moreover, it occupies the half of the cavity and some isotherms are also concentrated around the centered ellipse as it was heat absorbed. For $Re = 100, 500, 1000$ the vertical heat gradient near the left wall but in case of $Re = 2000$ near the right wall increased compared to previous case. Thus, in case of $\Delta = -3$ the temperature in the cavity increased compare to the previous one.
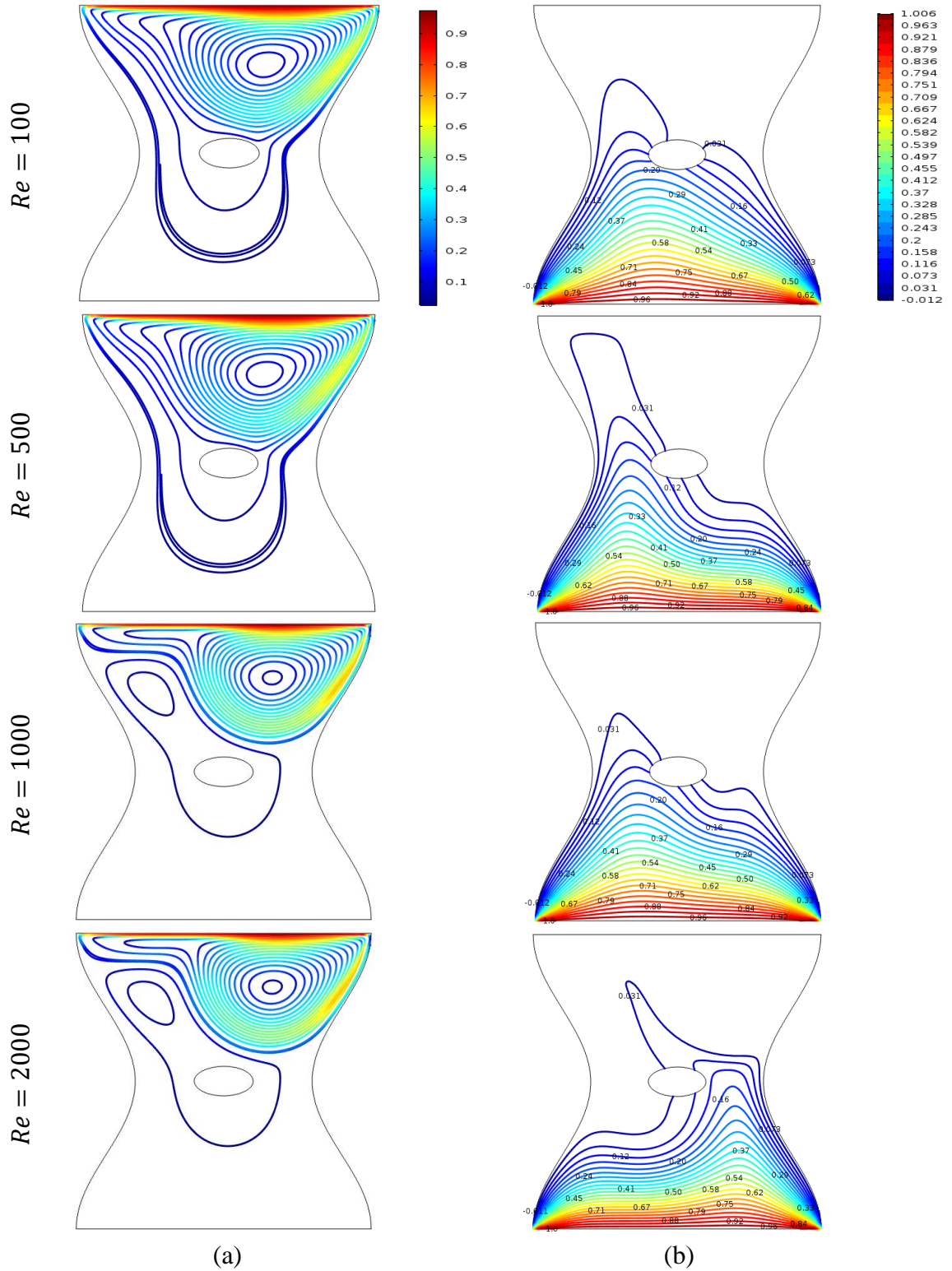
**Figure 4.2:** Effect of Reynolds number on (a) streamlines and (b) isotherms for $Pr = 0.70, \lambda = 1, Ha = 20, Gr = 10^4 \; and \; \Delta = -3.$

**4.2.3 Effect of Reynolds Number for Heat Generation ($\Delta = 3$)**



(a)                    (b)

**Figure 4.3:** Effect of Reynolds number on (a) streamlines and (b) isotherms for $Pr = 0.70, \lambda = 1, Ha = 20, Gr = 10^4 \ and \ \Delta = 3$.

The effects of Reynold's number $Re$ (= $100, 500, 1000, 2000$) on streamlines and isotherms in the present heat generation $\Delta = 3$ has been demonstrated in Figure 4.3(a)–(b). Reynold number represents the relative importance of mixed convection or combined forced convection and free convection. From Figure 4.3(a), it is seen that when $Re = 100$ the strength of buoyancy force inside the cavity is significant and a minor vortex is formed at left corner of the cavity but when $Re = 500$ there is only one vortex inside the cavity. Further again when Reynold's number increases ($Re = 1000$ and $2000$), the strength is more significant and two vortices appear. For $Re = 1000$ the secondary vortex appears to right cold wall with more cells. Again, for $Re = 2000$ the secondary vortex appears near the left cold wall and the cell enclosed the heat generation body.

From Figure 4.3(b)), we observed that the contour lines got densed near the bottom wall whereas distorted isotherms are distributed in the upper portion of the cavity for $Re = 100$. The isotherm patterns are quite similar for $Re = 500, Re = 1000$ $and$ $Re = 2000$. The vertical heat gradient takes part near the left wall. In addition, the isotherms are effectively close toward the hot wall as $Re$ is increased. At each increment in Reynolds numbers, there is a clear changed in isotherms distribution compared to previous one.

### 4.2.4 Effect of Reynolds Number for Heat Generation ($\Delta = 6$)

The effects of Reynolds number $Re$ (= $100, 500, 1000, 2000$) on streamlines and isotherms for the present configuration at $Ha = 20, Pr = 0.70, A = 0.1, \Delta = 6$ and $\lambda = 1$ has been demonstrated in Figure 4.4(a)–(b). From Figure 4.4 (a), we observed three vortices appear inside thecavity in which the major vortex contains a major vortex and another one is a minor vortex for $Re = 100$. But when $Re = 500$ there is only one vortex which covered almost whole cavity. Further again when $Re$ number increases to 1000 the strength of the buoyancy force is more significant and two vortices appear in which secondary vortex contains only one cell. For $Re = 2000$ the flow structure is similar to the case $\Delta = 3$. The physical fact behind it's that the greater effect of the Reynolds number increases the buoyancy force to influence the flow field.

Figure 4.4(b) express that isotherms appear in the entire cavity undergo noticeable distortion for $Re = 100$. With the increase of Reynolds numbers $Re = 500, 1000$ and $2000$, the intensity of heat transfer becomes higher and thus the isotherms appears in the entire cavity undergo noticeable vertical heat gradient takes part near the left wall. This vertical heat gradient in the isotherm contours indicates strong convection at higher Reynolds numbers.

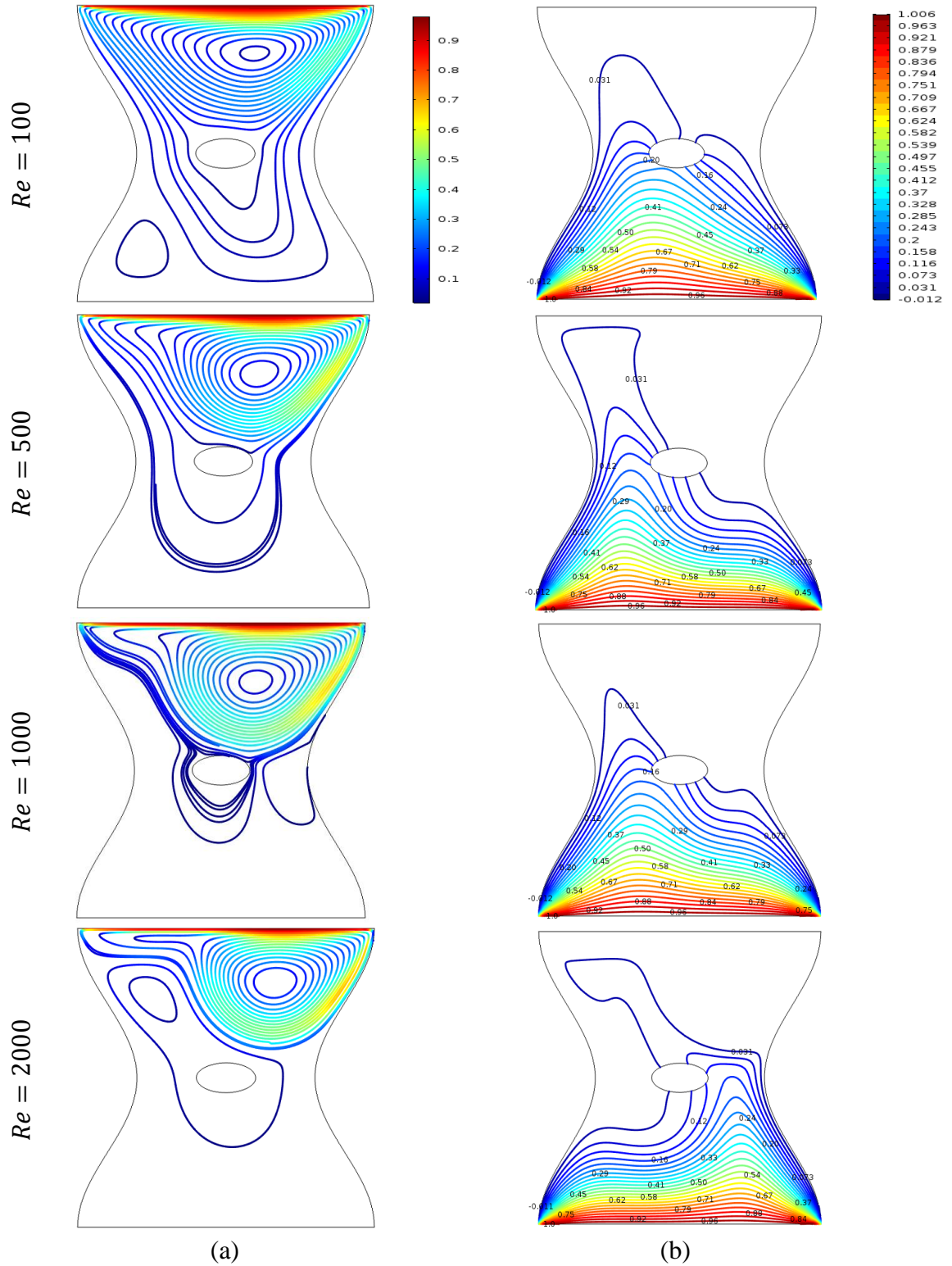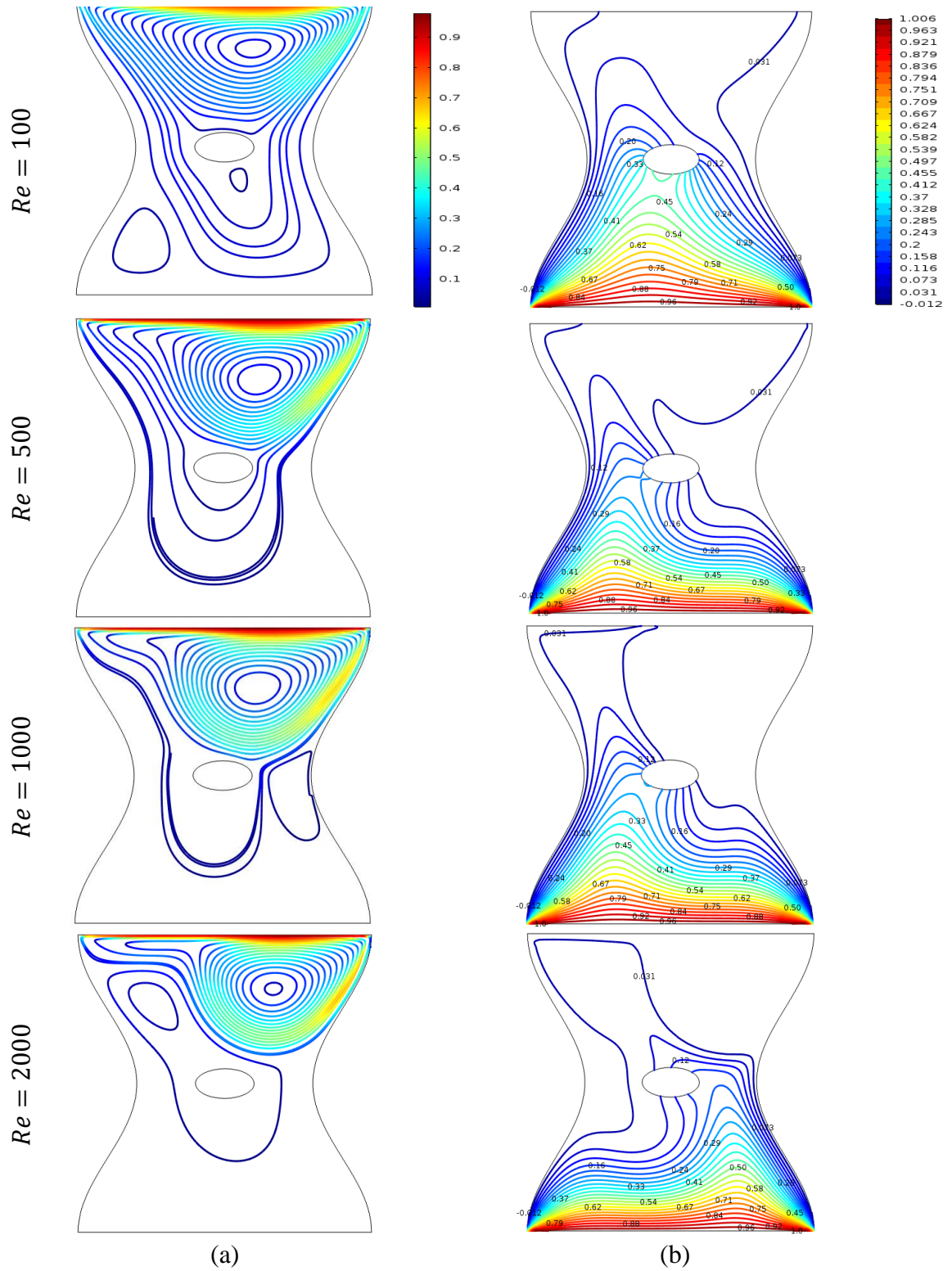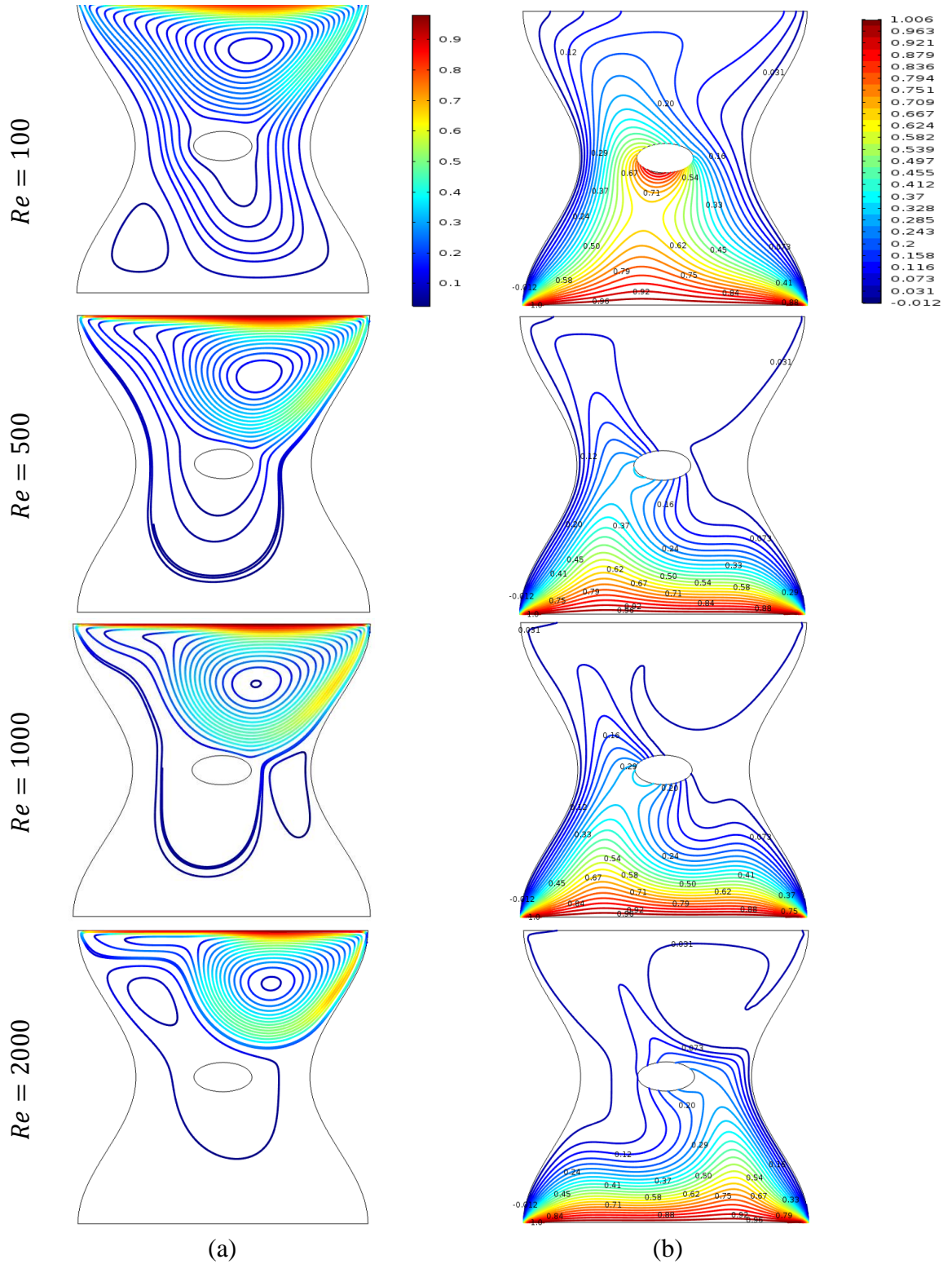**Figure 4.4:** Effect of Reynolds number on (a) streamlines and (b) isotherms for $Pr = 0.70, \lambda = 1, Ha = 20, Gr = 10^4 \ and \ \Delta = 6.$

### 4.2.5 Heat Transfer Rates

In this section, results of the numerical investigation of the effect of internal heat generator and absorption mixed convection heattransfer in presence of magnetic field in a lid-driven wavy cavity are numerically presented. The average Nusselt number and average fluid temperature against Reynold's numbers and heat absorption and generation are shown in Figure 4.5-4.6. Also, the heat transfer rates are given in the following Table 4.1-4.2.

**Table 4.1:** Numerical values of average Nusselt number against $Re$ on the bottom heated wall for selected value $\Delta$ while $Pr = 0.70, \lambda = 1, Ha = 20, Gr = 10^4$.

| $\Delta$ | Average Nusselt Number | | | |
|---|---|---|---|---|
| | Re = 100 | Re = 500 | $Re = 1000$ | $Re = 2000$ |
| -6 | 6.4419 | 6.4685 | 6.5054 | 6.9401 |
| -3 | 6.4356 | 6.4966 | 6.5625 | 7.0018 |
| 3 | 6.3982 | 6.6769 | 6.8249 | 7.1404 |
| 6 | 6.3253 | 6.9140 | 6.9648 | 7.2075 |
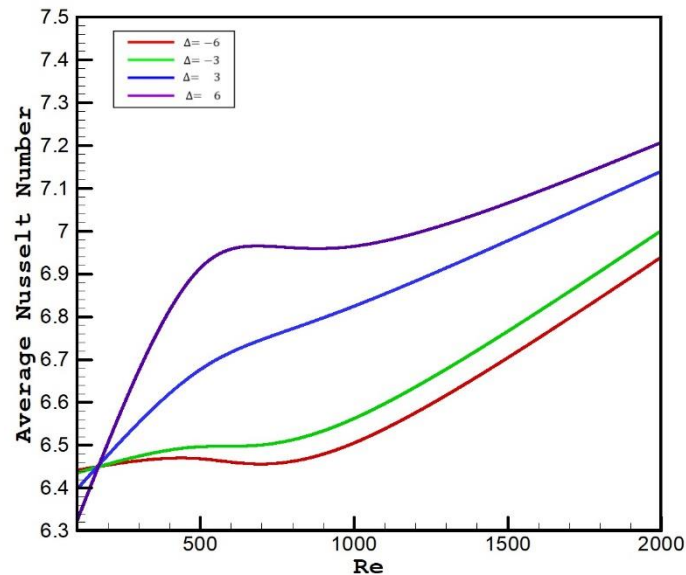


**Figure 4.5:** Variation of average Nusselt number of the heated bottom wall with Reynolds numbers for selected value $\Delta$ while $Pr = 0.70, \lambda = 1, Ha = 20, Gr = 10^4$.

Figure 4.5, illustrate that the average Nusselt number $(Nu_{av})$versus Reynolds numberalong the heated bottom wall for heat absorption and generation and $Pr = 0.70$ while the value of the remaining parameters is kept fixed. It can beseen from this Figure 4.5, the average Nusselt number increases when the value of the Reynolds number increases. At a constant Reynolds number, with increase in $\Delta$ the heat transfer is enhanced.

43

**Table 4.2:** Numerical values of average fluid temperature against $Re$ for selected value $\Delta$ while $Pr = 0.70, \lambda = 1, Ha = 20, Gr = 10^4$.

| $\Delta$ | Average Fluid Temperature | | | |
|:---:|:---:|:---:|:---:|:---:|
| | Re = 100 | Re = 500 | Re = 1000 | Re = 2000 |
| -6 | 1.5124 | 1.5131 | 1.5367 | 1.5592 |
| -3 | 1.5255 | 1.5379 | 1.5488 | 1.5767 |
| 3 | 1.6155 | 1.6189 | 1.6311 | 1.6327 |
| 6 | 1.6837 | 1.6910 | 1.6946 | 1.6989 |

Figure 4.6, illustrate that the average fluid temperature $(\theta_{av})$ versus Reynolds number $(Re)$ for various values of $\Delta$ while the value of the remaining parameters is kept constant. It can be seen from this Figure 4.6; average fluid temperature increases when the value of $\Delta$ increases at constant Reynolds number. It is also seen from this Figure 4.6; average fluid temperature increases with increasing $Re$ number.
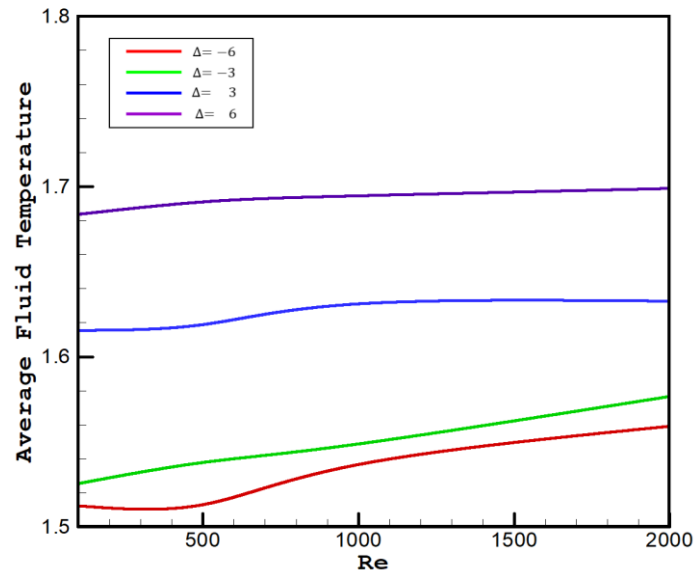


**Figure 4.6:** Variation of average temperature of fluid inside the cavity with Reynolds numbers for selected value $\Delta$ while $Pr = 0.70, \lambda = 1, Ha = 20, Gr = 10^4$.

Table 4.1 - 4.2, represent the values of the average Nusselt number and average fluid temperature respectively for considered parameters including $\Delta, Re\ Gr$ and $Pr$ respectively. Both the numerical result indicates that the average Nusselt number and average fluid temperature increases with increasing the value of $\Delta$.

Finally, both heat transfer rate and average temperature increase with increasing of $\Delta$ for all values of Reynolds number. At a constant $\Delta$, with an increase in Reynolds number heat transfer is enhanced for the entire regime.

## 4.3 EFFECT OF GRASHOF NUMBER

In this section, now discuss the performance of the Grashof number via streamline and isotherm contours and average Nusselt number by considering the heat generation and absorption while the Reynolds number is kept constant. In fact, the analysis is performed on mixed convection regime by fixing $Re = 100$. Four Grashof numbers $Gr = 10^3, 10^4, 10^5$ and $10^6$ at $Re = 100$ are chosen to examine the evolution of streamline, isotherm and average Nusselt number in presence of heat generation and absorption $\Delta = -6, -3, 3, 6$. The results of this parametric study are shown in Figure 4.7- 4.12.

### 4.3.1 Effect of Grashof Number for Heat Absorption ($\Delta = -6$)

The influence of Grashof number at constant Reynolds number in presence of heat absorption and generation on the flow and thermal fields are now investigated. Streamline and isotherm contours are plotted in Figure 4.7 for $Ha = 20, Pr = 0.70, A = 0.1, \Delta = 6$ and $\lambda = 1$. At $Gr = 10^3$, the streamline pattern (see Figure 4.7 (a)) consists of a large lid-driven clockwise vortex in the top of the cavity but in case of $Gr = 10^4$ a smaller vortex appears in the left bottom side of the cavity with single circulation. For $Gr = 10^5 \ and \ 10^6$, flow pattern is usual with four vortices in the cavity. There is a difference in the streamline contours observed for $Gr = 10^6$. When the Grashof number increases, the number of vortices in the cavity increased with an increased strength. The difference of the streamline patterns appears dominantly at higher $Gr$.

The isotherm patterns are quite similar for $Gr = 10^3 \ and \ Gr = 10^4$ (see Figure 4.7 (b)). The contour lines are clustered near the bottom wall. With the increase of Grashof numbers $Gr = 10^5 \ and \ Gr = 10^6$, the intensity of free convection heat transfer becomes higher and thus the isotherms appears in the entire cavity undergo noticeable distortion. This distortion in the isotherm contours indicates strong convection at higher Grashof numbers. However, change in isotherm pattern for high Grashof numbers is significant.

**Figure 4.7:** Effect of Grashof number on (a) streamlines and (b) isotherms for $Pr = 0.70, \lambda = 1, Ha = 20, Re = 10^2$ and $\Delta = -6$.

**4.3.2 Effect of Grashof Number for Heat Absorption ($\Delta = -3$)**



**Figure 4.8:** Effect of Grashof number on (a) streamlines and (b) isotherms for $Pr = 0.70, \lambda = 1, Ha = 20, Re = 10^2$ and $\Delta = -3$.

The influence of Grashof number at constant Reynolds number in presence of heat absorption and generation on the flow and thermal fields are now investigated. Streamline and isotherm contours are plotted in Figure 4.8 for $Ha = 20, Pr = 0.70, A = 0.1, \Delta = 3$ and $\lambda = 1$. At $Gr = 10^3$, the streamline pattern (see Figure 4.8 (a)) consists of a large lid-driven clockwise vortex in the top of the cavity but in case of $Gr = 10^4$ there are three vortices included a large lid-driven clockwise vortex in the top of the cavity, a singled cell vortex bellows the heat absorption term and smaller vortex appears in the left bottom side of the cavity with single circulation. For $Gr = 10^5$ flow pattern appears with four vortices in the cavity. There are five contours in the streamline observed for $Gr = 10^6$. When the Grashof number increases, the number of vortices in the cavity increased with an increased strength. The difference of the streamline patterns appears dominantly at higher $Gr$.

The isotherm patterns are quite similar for $Gr = 10^3 and Gr = 10^4$ (see Figure 4.8 (b)). The contour lines are clustered near the bottom wall. With the increase of Grashof numbers $Gr = 10^5 \ and \ Gr = 10^6$, the intensity of free convection heat transfer becomes higher and thus the isotherms appears in the entire cavity whereas distorted isotherms are distributed in the upper portion of the cavity. This distortion in the isotherm contours indicates strong convection at higher Grashof numbers. However, change in isotherm pattern for high Grashof numbers is noticeable.
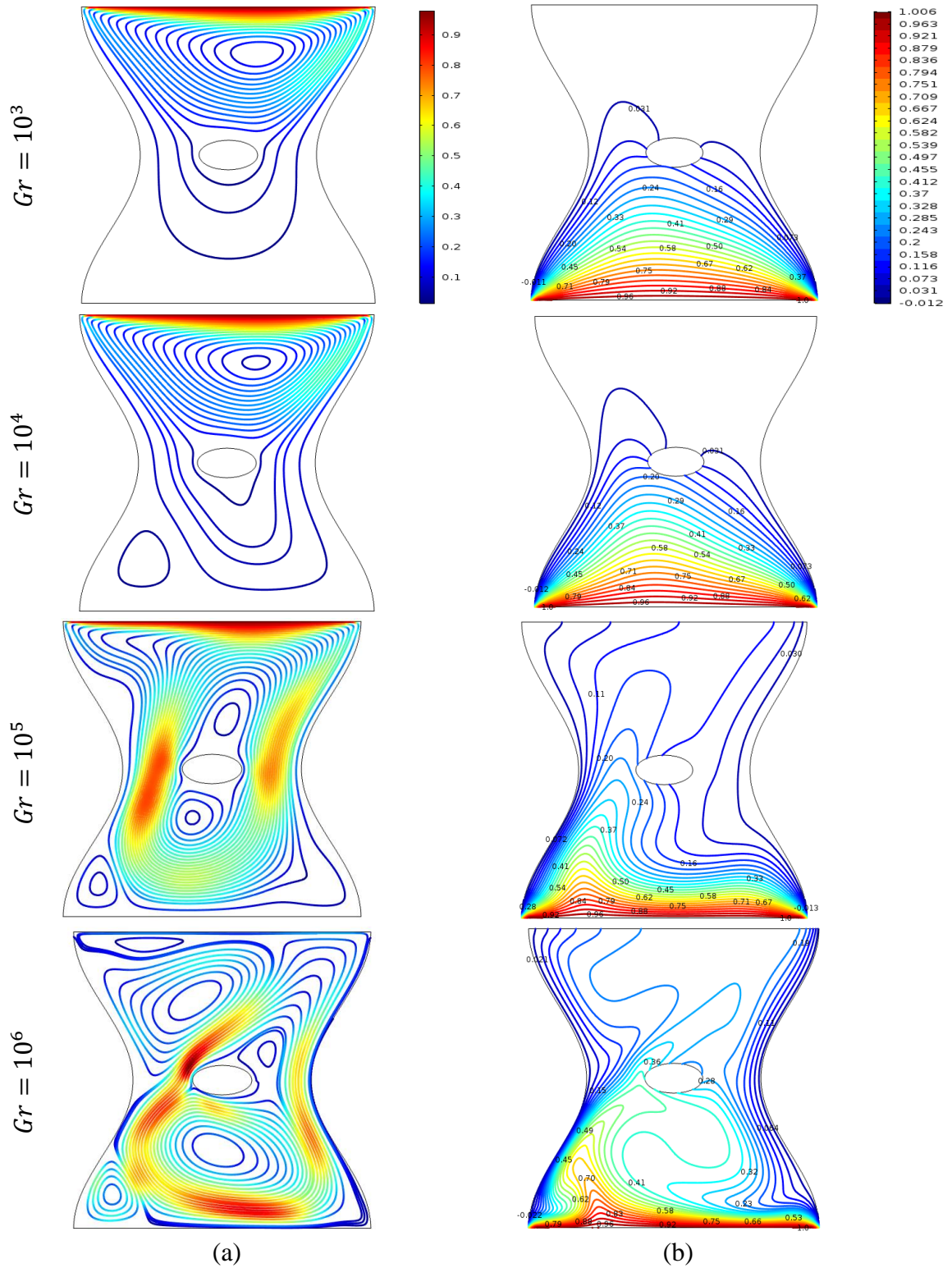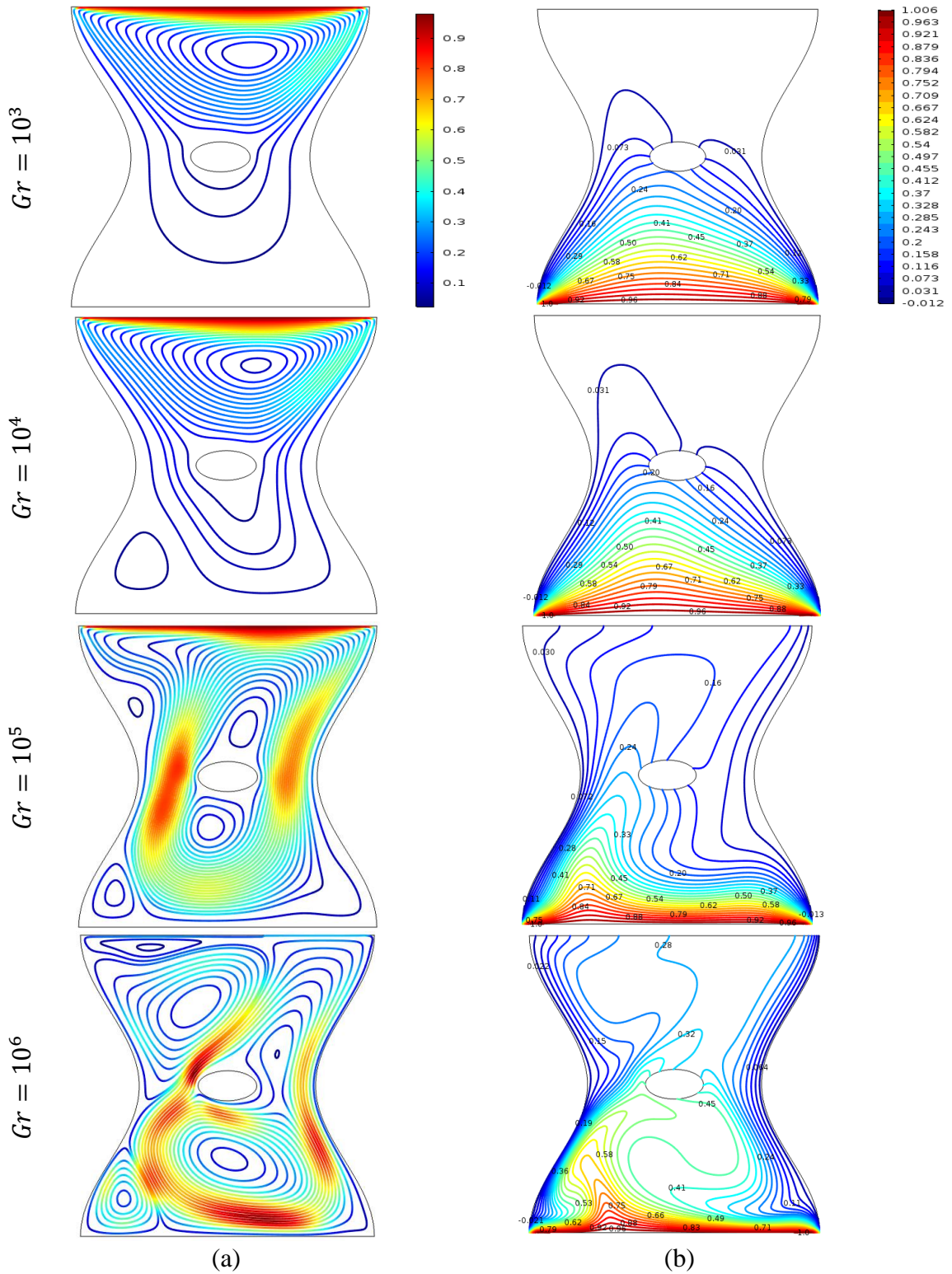
### 4.3.3 Effect of Grashof Number for Heat Generation ($\Delta = 3$)

The influence of Grashof number at constant Reynolds number in presence of heat absorption and generation on the flow and thermal fields are now investigated. Streamline and isotherm contours are plotted in Figure 4.9((a)-(b)) for $Ha = 20, Pr = 0.70, A = 0.1, \Delta = 3$ and $\lambda = 1$. For $Gr = 10^3$, the streamline pattern (see Figure 4.9 (a)) consists of a large lid-driven clockwise vortex in the top of the cavity with more cells than previous case. At $Gr = 10^4$ there is a primary vortex in the top of the cavity and a smaller vortex appears in the left bottom side of the cavity with single circulation. For $Gr = 10^5 \ and \ 10^6$, flow pattern is usual with four vortices in the cavity. There is a difference in the streamline contours observed for $Gr = 10^6$. When the Grashof number increases, the number of vortices in the cavity increased with an increased strength. The difference of the streamline patterns appears dominantly at higher $Gr$.
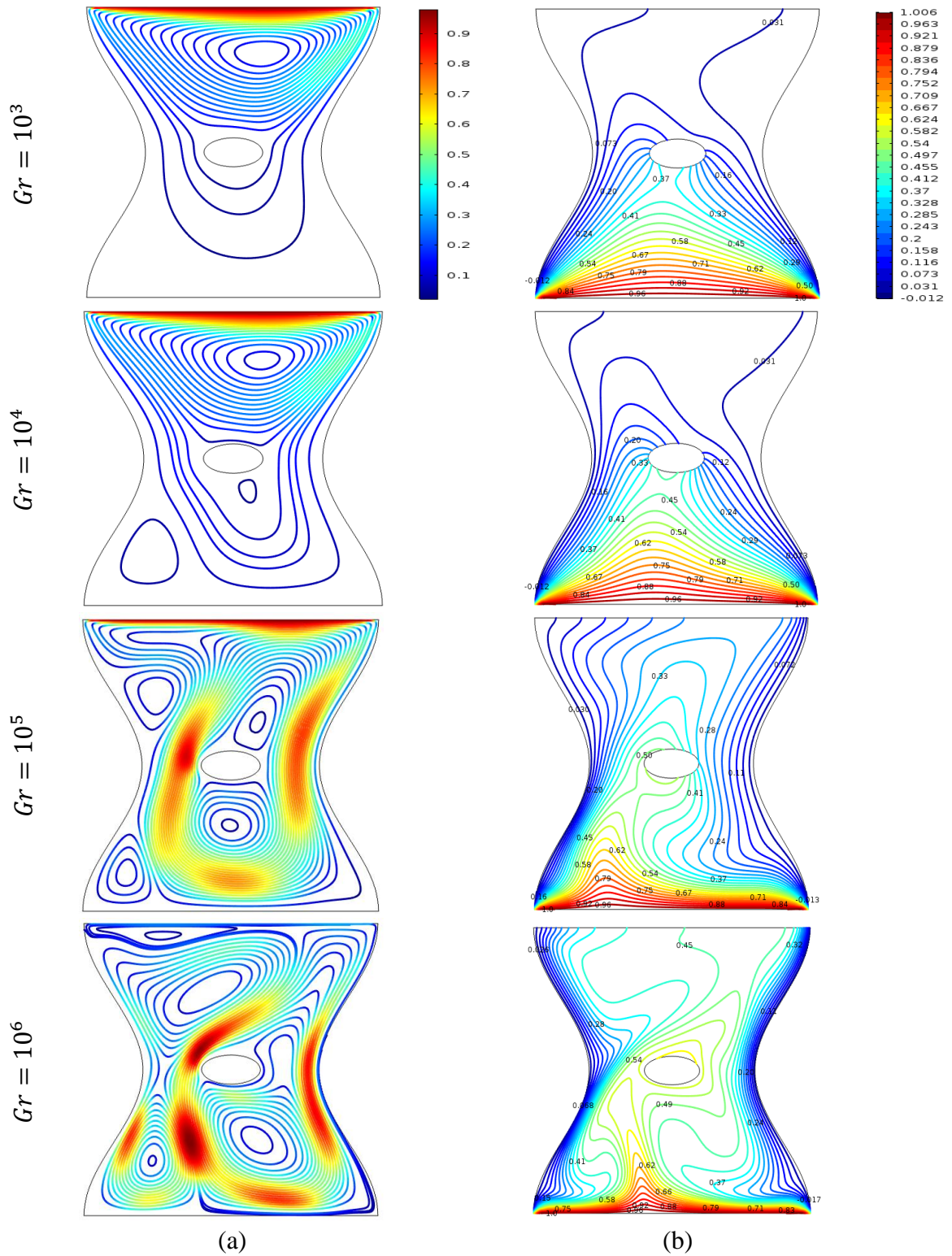
**Figure 4.9:** Effect of Grashof number on (a) streamlines and (b) isotherms for $Pr = 0.70, \lambda = 1, Ha = 20, Re = 10^2$ and $\Delta = 3$.

The isotherm patterns for $Gr = 10^3$ (see Figure 4.9 (b)) consists of a contour line are clustered near the bottom wall whereas distorted isotherms are distributed in the upper portion of the cavity in the case $Gr = 10^4$. The isotherm patterns are quite similar for $Gr = 10^5$ $and$ $Gr = 10^6$, the isotherms appear in the entire cavity undergo noticeable distortion. This distortion in the isotherm contours indicates strong convection at higher Grashof numbers. The intensity of heat transfer becomes higher with the increase of $Gr$ at $\Delta = 3$.

### 4.3.4 Effect of Grashof Number for Heat Generation ($\Delta = 6$)

The effect of Gr on streamline and isotherm contours are plotted in Figure 4.10(a)-(b) for $Ha = 20, Pr = 0.70, A = 0.1, \Delta = 6$ and $\lambda = 1$. At $Gr = 10^3$, the streamline pattern (see Figure 4.10 (a)) consists of a large lid-driven clockwise vortex in the top of the cavity with increase cell distance than the case $\Delta = 3$. When the Grashof number increases in presence of heat generation $\Delta = 6$, the number of vortices in the cavity increased with an increased strength. We observed three vortices appear inside the cavity. For $Gr = 10^5$ $and 10^6$ , flow pattern is usual with four vortices in the cavity. There is difference in the streamline contours observed for $Gr = 10^6$. The difference of the streamline patterns appears dominantly at higher $Gr$.

The isotherm patterns are quite similar for $Gr = 10^3$ $and$ $Gr = 10^4$ (see Figure 4.10 (b)). The contour lines are clustered near the bottom wall whereas distorted isotherms are distributed in the upper portion of the cavity. With the increase of Grashof numbers $Gr = 10^5$ $and$ $Gr = 10^6$, heat transfer becomes higher and thus the isotherms appears in the entire cavity undergo noticeable distortion. This distortion in the isotherm contours indicates strong convection at higher Grashof numbers.
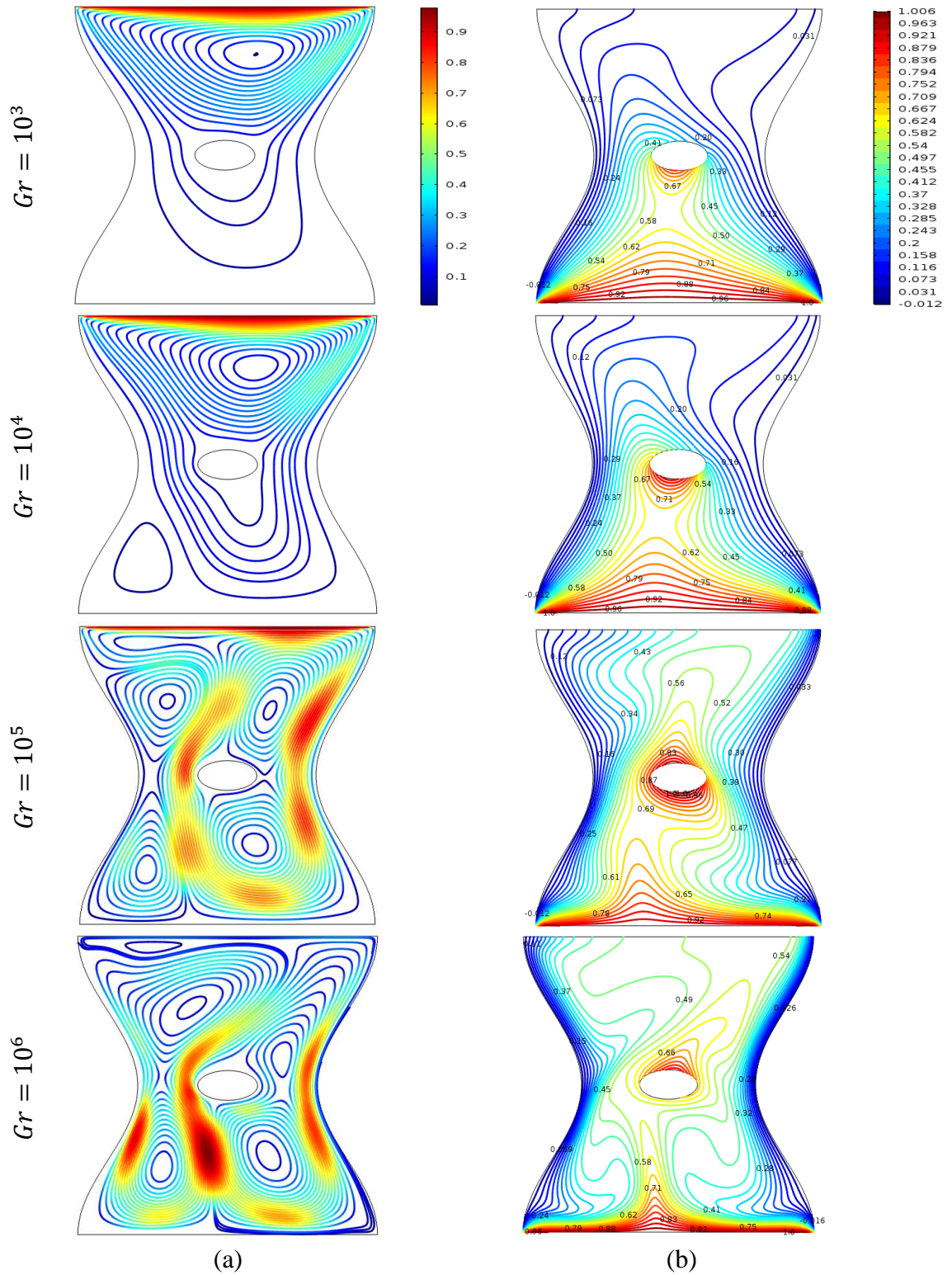
**Figure 4.10:** Effect of Grashof number on (a) streamlines and (b) isotherms for $Pr = 0.70, \lambda = 1, Ha = 20, Re = 10^2$ and $\Delta = 6$.

### 4.3.5 Heat Transfer Rates

In this section, outcomes of the numerical experiment of the impact of internal heat generator or absorption mixed convection heat transfer in presence of magnetic field in a lid-driven wavy cavity are numerically illustrated. The average Nusselt number and average fluid temperature against Grashof numbers and heat absorption and generation are shown in Figure 4.11-4.12. Also, the heat transfer rates are given in the following Table 4.3-4.4.

**Table 4.3:** Numerical values of average Nusselt number against $Gr$ on the bottom heated wall for selected value $\Delta$ while $Pr = 0.70, \lambda = 1, Ha = 20, Re = 10^2$.

| $\Delta$ | Average Nusselt Number | | | |
|---|---|---|---|---|
| | $Gr = 10^3$ | $Gr = 10^4$ | $Gr = 10^5$ | $Gr = 10^6$ |
| -6 | 6.3934 | 6.4419 | 7.8811 | 12.4753 |
| -3 | 6.3784 | 6.4356 | 7.9306 | 12.4861 |
| 3 | 6.3009 | 6.3982 | 8.1076 | 12.7786 |
| 6 | 6.1295 | 6.3253 | 8.1532 | 12.8192 |
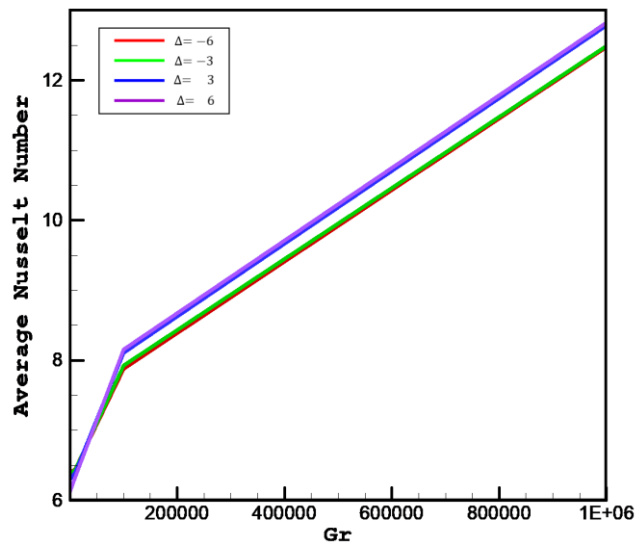


**Figure 4.11:** Variation of average Nusselt number of the heated bottom wall with Grashof number for selected value $\Delta$ while $Pr = 0.71, \lambda = 1, Ha = 20, Re = 10^2$.

Figure 4.11 depict the average Nusselt number $(Nu_{av})$ versus Grashof number along the heated bottom wall for heat absorption or generation while the value of the remaining parameters is kept specified. It can be noticed from this figure, the average Nusselt number advances when the value of the Grashof $Gr$ number advances. At a fixed Grashof number, with the boost in $\Delta$ the heat transfer is enhanced.

Figure 4.12 illustrate that the average fluid temperature versus Grashof number for various values of while the value of the remaining parameters is kept constant. It can be seen from this figure; average fluid temperature increases when the value of Grashof increase at a constant value of $\Delta$. It is also seen from this figure; average fluid temperature increases steadily with increasing value of Grashof number when $\Delta$ is kept constant.

Figure 4.12 demonstrate the average fluid temperature$(\theta_{av})$ versus Grashof number$(Gr)$ for various values of $\Delta$ while the value of the remaining parameters is kept invariant. It can be noticed from this figure; average fluid temperature improves when the value of Grashof increase at a constant value of $\Delta$. It is also observed from this figure; average fluid temperature expands steadily with the increasing value of Grashof number when $\Delta$ is remaining fixed.

**Table 4.4:** Numerical values of average fluid temperature against $Gr$ for selected value $\Delta$ while $Pr = 0.71, \lambda = 1, Ha = 20, Re = 10^2$.

| $\Delta$ | Average Fluid Temperature | | | |
|---|---|---|---|---|
| | $Gr = 10^3$ | $Gr = 10^4$ | $Gr = 10^5$ | $Gr = 10^6$ |
| -6 | 1.4860 | 1.5124 | 1.7936 | 2.1680 |
| -3 | 1.4939 | 1.5255 | 1.8241 | 2.2129 |
| 3 | 1.5666 | 1.6355 | 2.1210 | 2.5435 |
| 6 | 1.8670 | 2.0491 | 2.7338 | 2.7276 |
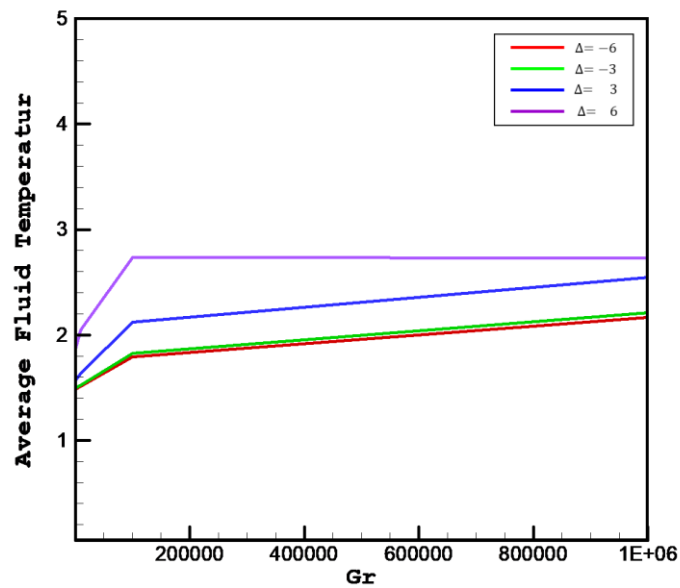


**Figure** 4**.12:** Variation of average temperature of fluid inside the cavity with Grashof for selected value $\Delta$ while $Pr = 0.70, \lambda = 1, Ha = 20, Re = 10^2$.

Table 4.3 - 4.4 describe the values of the average Nusselt number and average fluid temperature respectively for supposed parameters including $Ri, Pr, Gr, Re$ and $\Delta$ respectively. Both the numerical outcome signifies that the average Nusselt number and average fluid temperature increases with improving the value of $Gr$ and $\Delta$.

Eventually, both heat transfer rate and average temperature boost with increasing of Grashof number for all values of $\Delta$. At a fixed Grashof number, with the expansion in $\Delta$ the buoyancy force increases and heat transfer is enhanced.

## 4.4 EFFECT OF RICHARDSON NUMBER

In this section, the characteristics of the flow and temperature fields in the lid driven cavity having one undulation are examined by exploring the effects of the Richardson number Ri, in presence of heat generation and absorption coefficient $\Delta$. Such field variables are examined by outlaying the steady state version of the streamlines and temperature distributions as well as the average Nusselt number $Nu_{av}$. In the current numerical investigation, the following parametric domains of the dimensionless groups are considered: $Ri = 0.1, 1, 5, 10, Ha = 20$, $\Delta = -6, -3, 3, 6$, $Re = 100$ and $Pr = 0.7$. The results of this parametric study are shown in Figure 4.13- 4.18.

### 4.4.1 Effect of Richardson Number for Heat Absorption ($\Delta = -6$)

Figure 4.13((a)-(b)) demonstrated the performance of Richardson number in presence of heat absorption $\Delta = -6$ via streamline and isotherm contours by considering $Re = 100$. In fact, the analysis is performed at Richardson number $Ri = 0.1, 1, 5, 10$ and the corresponding value of Reynolds number Re = 100. When $Ri = 0.1, 1$ there is only one vortex inside the top of the cavity. The clockwise rotating vortex induced by the moving lid is dominant. For $Ri = 5$, the lid-driven vortex expands towards the bottom part of the cavity and grows larger and there are three vortices having opposite sense of rotation. The primary vortex includes a secondary vortex with two contours at the below of the heat generation term and another secondary vortex appears at the left corner of the cavity. On the other hand, the streamlines cover the whole cavity with same vortices in the case $Ri = 10$ but streamline contours and flow strength increased compare to the cases $Ri = 5$. Which implies the fluid velocity increases with increasing value of $Ri$.

From Figure 4.13(b), we observed that the isotherms inside the cavity are found to undergo same changes due to the effect of $Ri = 0.1, 1$ in the case of internal heat absorption $\Delta = -6$, where the high temperature region moves closer to the hot base wall. Less energy is noticed to be carried away from the sliding top wall into the cavity and, subsequently, the conduction heat transfer regime has become the dominant mode of energy transport in the cavity as a result a strong thermal boundary layer develops near the bottom and left wall. It may be noted that the isotherm contour is extended toward the top adiabatic wall and there is temperature gradient for $Ri = 5$. Which implies heat convection increased with increasing $Ri$. In the case $Ri = 10$, isotherm pattern almost same as $Ri = 5$ but number of extended isotherm contour and temperature increased.

**Figure 4.13:** Effect of $Ri$ number on (a) streamlines and (b) isotherms for $Pr = 0.70, \lambda = 2, Ha = 20, Re = 100$ and $\Delta = -6$.

<p style="text-align:center">(a)               (b)</p>

**Figure 4.14:** Effect of $Ri$ number on (a) streamlines and (b) isotherms for $Pr = 0.70, \lambda = 2, Ha = 20, Re = 100$ and $\Delta = -3$.

Figure 4.14((a)-(b)) represented the performance of Richardson number in presence of heat absorption $\Delta = -3$ via streamline and isotherm contours by considering $Re = 100$. In fact, the analysis is performed at Richardson number Ri= 0.1, 1, 5, 10 and the corresponding value of

Reynolds number Re $= 100$. When $Ri = 0.1$, there is only one vortex inside the top of the cavity. For $Ri = 1$ the lid-driven vortex expands towards the bottom part of the cavity and grows larger and there are two vortices. The streamlines pattern is almost same as previous case for $Ri = 5$ but the flow strength increased in this case. On the other hand, when $Ri = 10$ there are four vortices inside the cavity in which the primary vortex includes a minor vortex and other two vortices are located near the left wall. Thus, the buoyancy force increases with increasing value of $Ri$ and $\Delta$.

From Figure 4.14(b), we observed that the isotherms inside the cavity are found to undergo same changes due to the effect of $Ri = 0.1, 1, 5, 10$ in the case of internal heat absorption $\Delta = -3$, as the previous cases but distorted isotherm contours and temperature gradient increased. Which implies that the heat transfer rate and internal temperature increased with increasing $Ri$ and $\Delta$.

### 4.4.3 Effect of Richardson Number for Heat Generation ($\Delta = 3$)

From Figure 4.15((a)-(b)), we observed the effect heat generation $\Delta = 3$ via streamline and isotherm contours by considering the effect of Richardson numbers while the Reynolds number is kept constant. For $Ri = 0.1$ there is only one vortex inside the top of the cavity. The clockwise rotating vortex induced by the moving lid is dominant. With the increase of $Ri$, the lid-driven vortex expands towards the bottom part of the cavity and grows larger and there are three vortices inside the cavity at $Ri = 1$. For $Ri = 5$, the number of distinct vortices inside the cavity are same as $Ri = 1$ but streamlines contour increased. On the other hand, the streamlines cover the whole cavity with four vortices with minimum cell distance in the case $Ri = 10$. Thus, the heat generation has great impact on flow strength and velocity.

The isotherm patterns are quite similar for $Ri = 0.1 \ to \ 1$, (see Figure 4.15(b)). The contour lines are clustered near the bottom wall whereas distorted isotherms are distributed in the upper portion of the cavity. With the increase of Richardson number $Ri = 5 \ to \ 10$ heat transfer becomes higher and thus the parallel distribution of isotherm contours breaks up and is distorted throughout the cavity. This distortion in the isotherm contours indicates significant difference for Richardson numbers and heat generation.
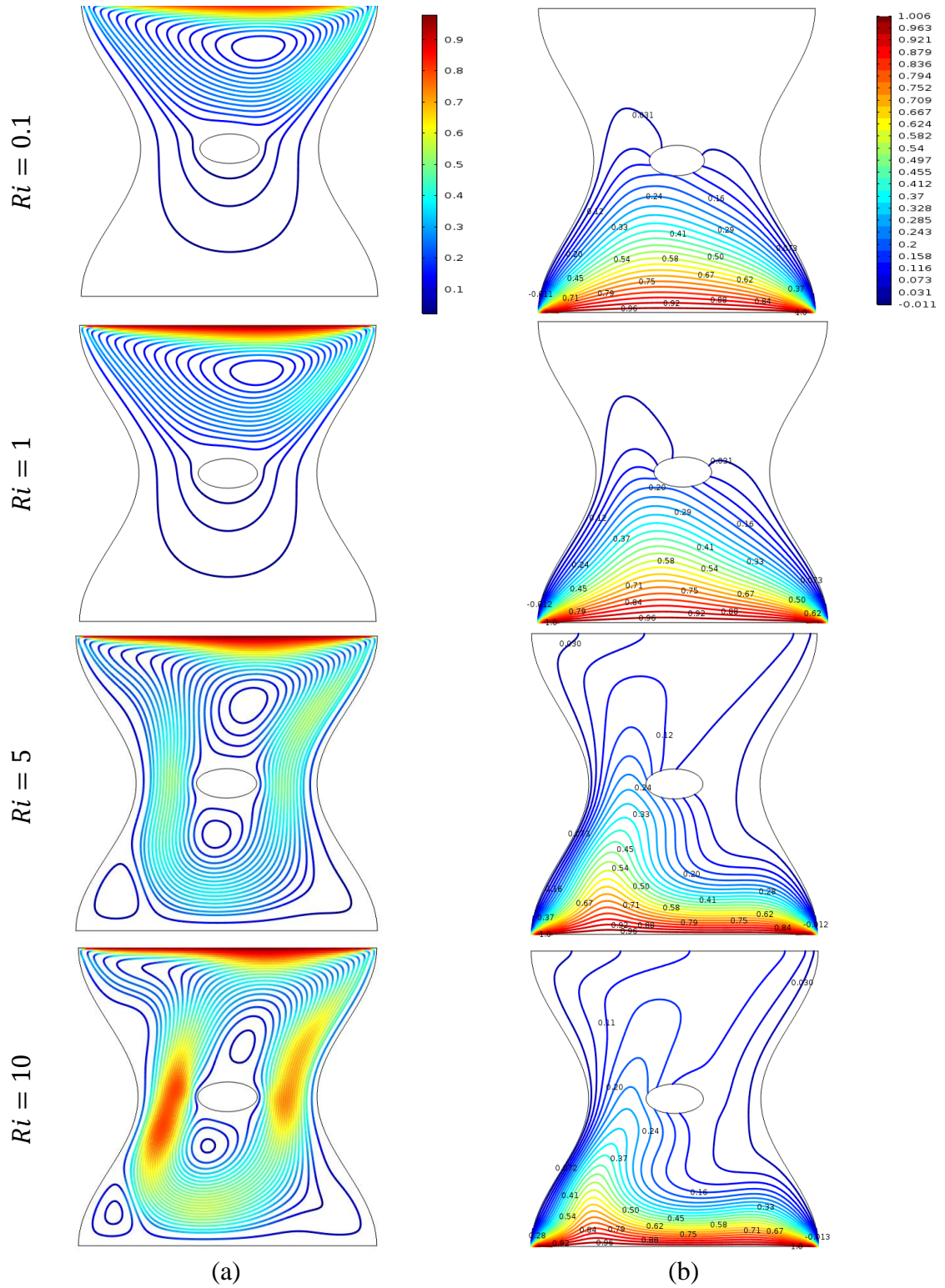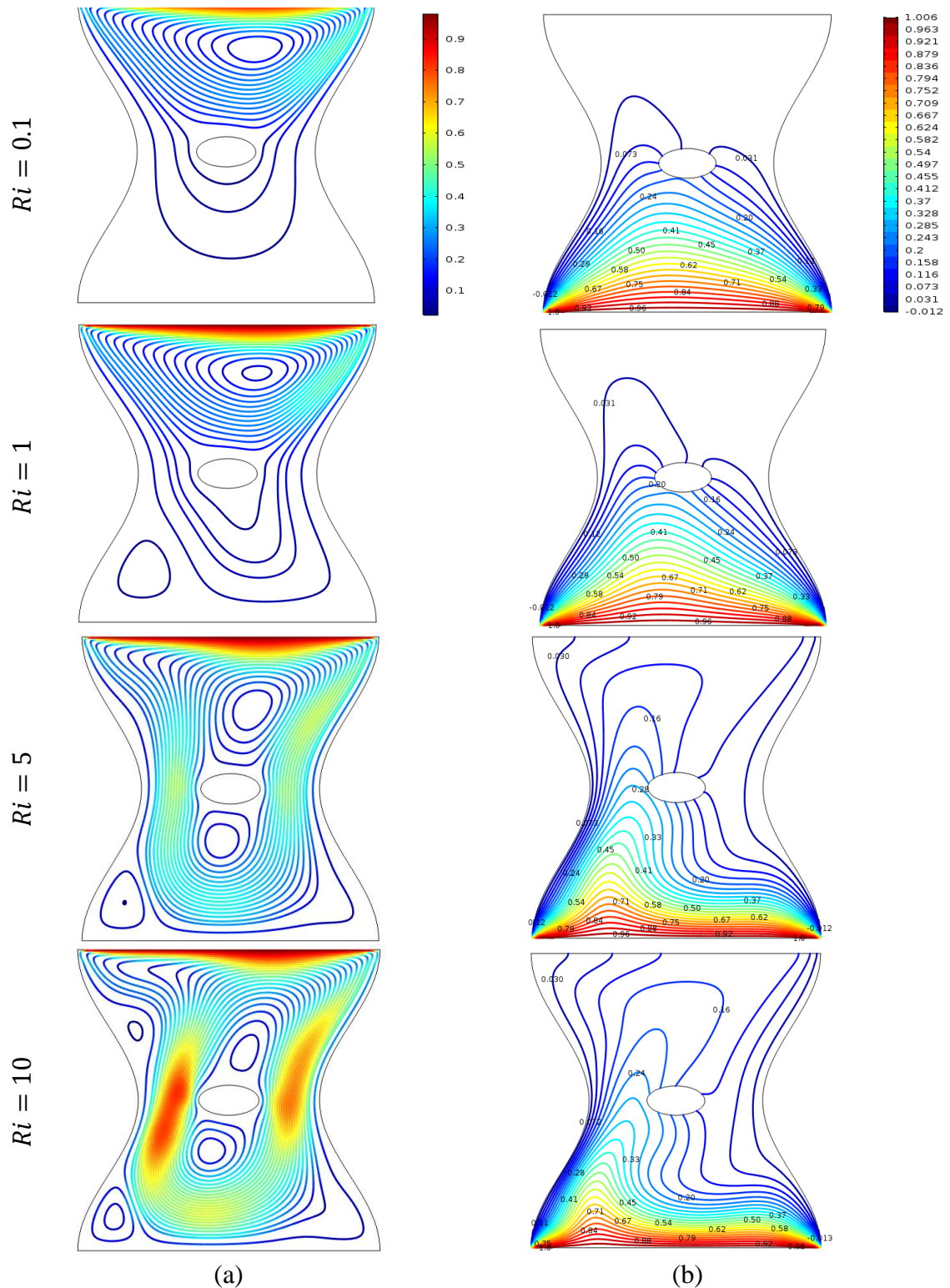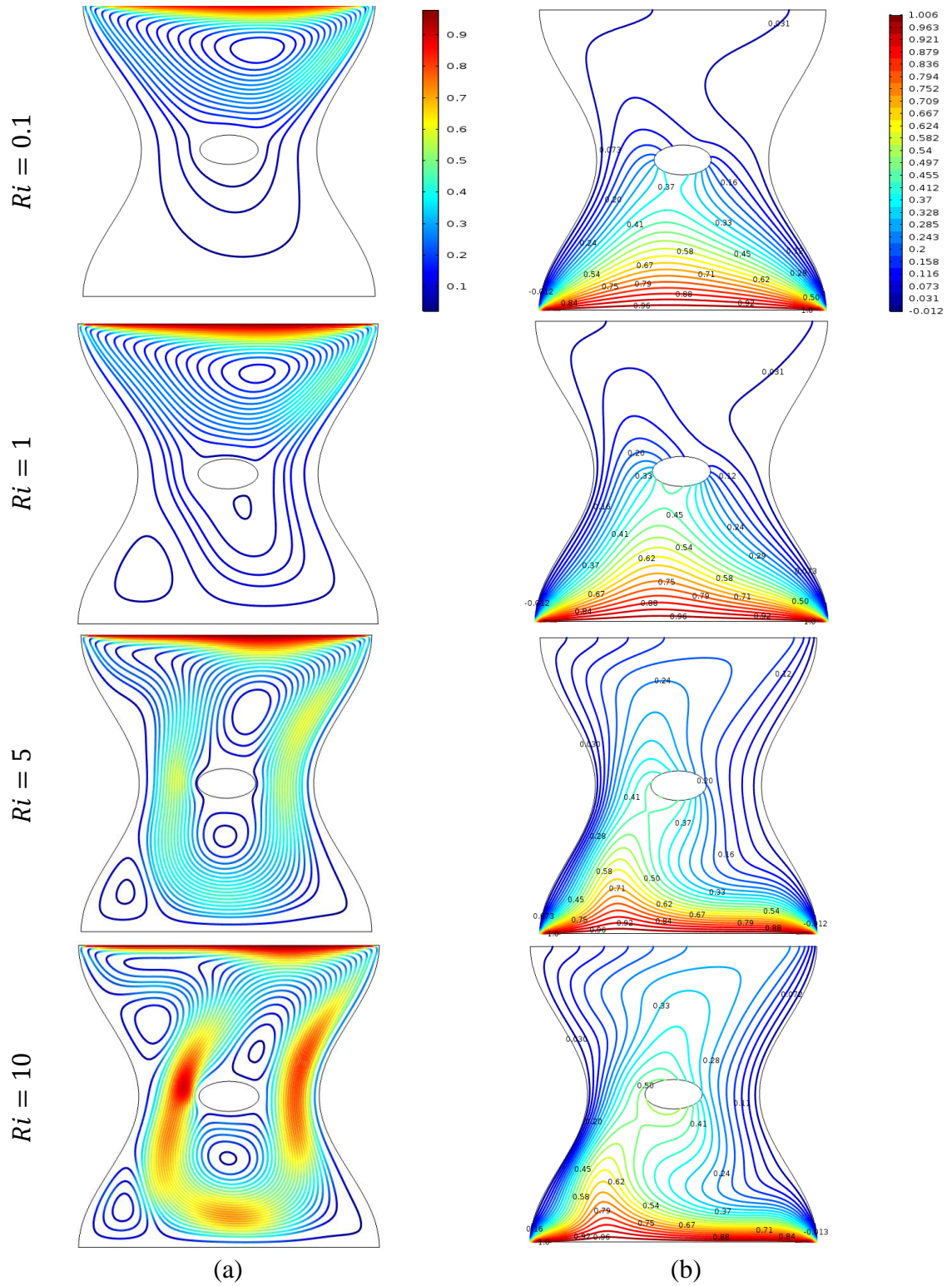
**Figure 4.15:** Effect of $Ri$ number on (a) streamlines and (b) isotherms for $Pr = 0.70, \lambda = 2, Ha = 20, \ Re = 100 \ and \ \Delta = 3$.

**4.4.4 Effect of Richardson number for Heat Generation ($\Delta = 6$)**



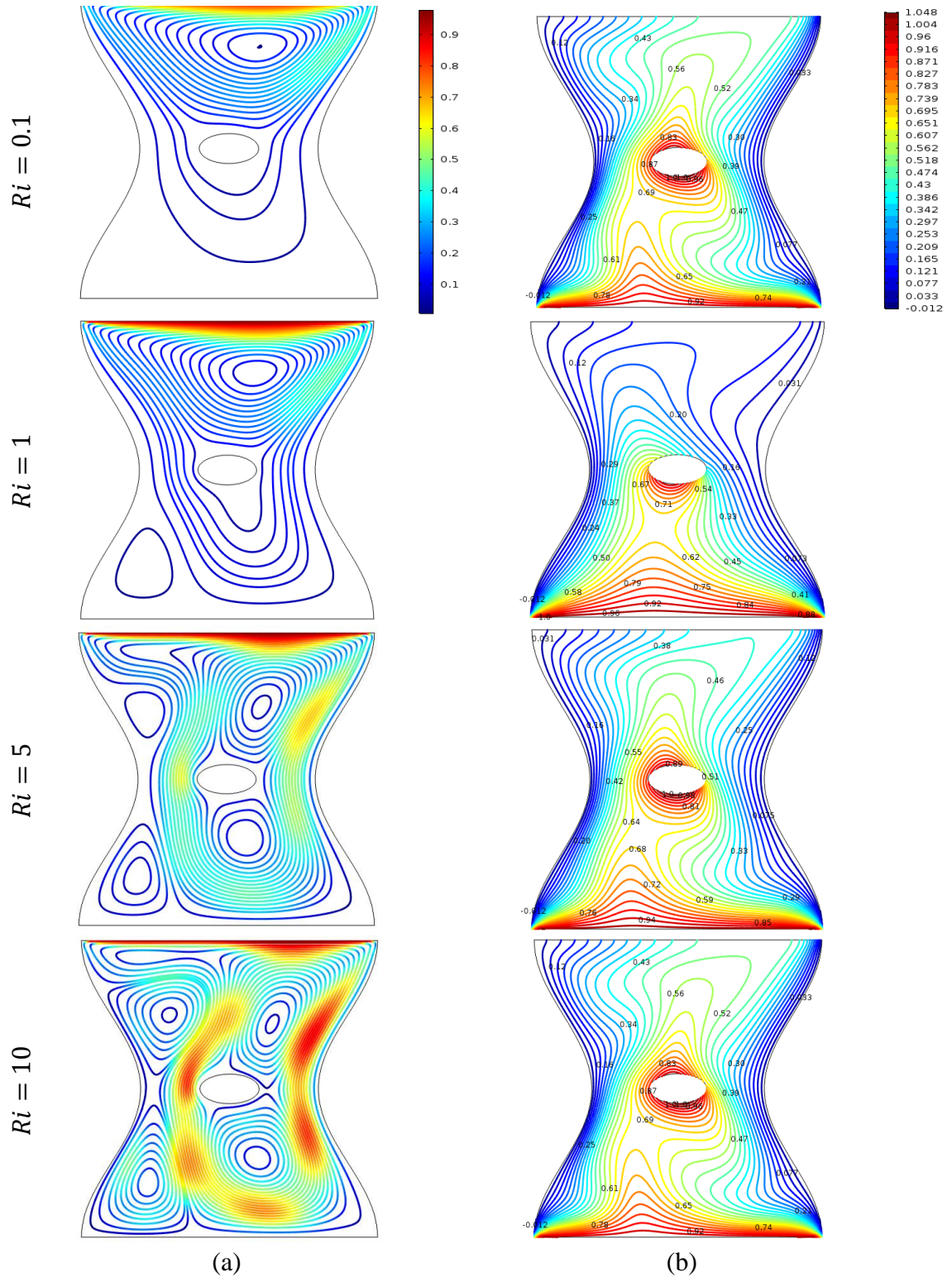**Figure 4.16:** Effect of $Ri$ number on (a) streamlines and (b) isotherms for $Pr = 0.70, \lambda = 2, Ha = 20, Re = 100$ $and$ $\Delta = 6$.

Figure 4.16(a), for $Ri = 0.1$ there is only one vortex inside the top of the cavity. The clockwise rotating vortex induced by the moving lid is dominant. For $Ri = 1$ the lid-driven vortex expands towards the bottom part of the cavity and grows larger and there are two vortices. For

$Ri = 5$, there are four distinct vortices inside the cavity having opposite sense of rotation. The primary vortex includes a secondary vortex at the below of the heat generation term and another two secondary vortices are at the left corner of the cavity. On the other hand, the streamlines cover the whole cavity with four vortices in the case $Ri = 10$ but stream line contour increased compare to the previous cases. Which implies the fluid velocity increases with increasing value of $Ri$.

The isotherms inside the cavity are found to undergo some changes due to the effect of $Ri = 0.1, 1, 5$ and 10 in the case of internal heat generation $\Delta = 6$ are represented in Figure 4.16. As the $Ri$ effect increases a localized region of high temperature is noticed in the core region and the high temperature region is extended toward the top adiabatic wall. This is due to the fact that the hot fluid cannot reject energy near the top adiabatic wall. This effect becomes clearer for the increasing values of Richardson number ($Ri$).

### 4.4.5 Heat Transfer Rates

In this section, consequences of the numerical investigation of the influence of $Ri$ on mixed convection heat transfer in presence of inner heat generator or absorption in a lid-driven cavity having single undulation are numerically presented. The average Nusselt number and average fluid temperature against Richardson number are shown in Figure 4.17-4.18. Also, the heat transfer rates are given in the following Table 4.5-4.6.

**Table 4.5:** Numerical values of average Nusselt number against $Ri$ on the bottom heated wall for selected value $\Delta$ while $Pr = 0.70, \lambda = 1, Ha = 20, Re = 100$.

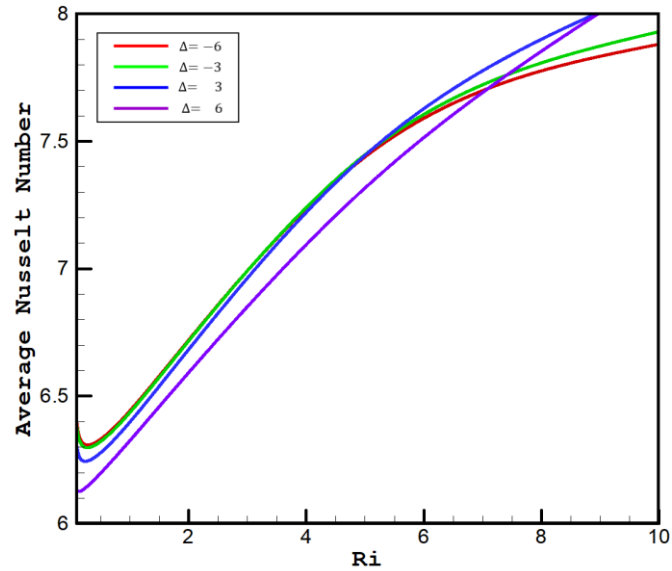| $\Delta$ | Average Nusselt Number | | | |
|---|---|---|---|---|
| | $Ri = 0.1$ | $Ri = 1$ | $Ri = 5$ | $Ri = 10$ |
| -6 | 6.3934 | 6.4419 | 7.4389 | 7.8811 |
| -3 | 6.3783 | 6.4356 | 7.4478 | 7.9305 |
| 3 | 6.3009 | 6.3982 | 7.4451 | 8.1076 |
| 6 | 6.1292 | 6.3253 | 7.3171 | 8.1534 |

**Figure 4.17:** Variation of the average Nusselt number against $Ri$ for selected value $\Delta$ while $Pr = 0.70, \lambda = 1, Ha = 20, Re = 100$.

**Figure 4.17** represent the average Nusselt number $(Nu_{av})$ versus Ricardson number along the heated bottom wall for heat absorption or generation while the value of the remaining parameters is kept specified. It can be noticed from this figure, the average Nusselt number improves when the value of the Richardson number improves. At a consistent Ricardson number, with an addition in $\Delta$ the heat transfer is declined.

**Table 4.6:** Numerical values of average fluid temperature against $Ri$ on the bottom heated wall for selected value $\Delta$ while $Pr = 0.70, \lambda = 1, Ha = 20, Re = 100$.

| $\Delta$ | Average fluid temperature | | | |
|---|---|---|---|---|
| | $Ri = 0.1$ | $Ri = 1$ | $Ri = 5$ | $Ri = 10$ |
| -6 | 1.4860 | 1.5124 | 1.7317 | 1.7936 |
| -3 | 1.4939 | 1.5255 | 1.7560 | 1.8241 |
| 3 | 1.5665 | 1.6355 | 1.9502 | 2.12095 |
| 6 | 1.8670 | 2.0491 | 2.5894 | 2.7338 |

Figure 4.18 describe that the average fluid temperature $(\theta_{av})$ versus    for various value of $\Delta$ while the value of the remaining parameters is kept stable. It can be seen from this Figure 4.18; average fluid temperature increases when the value of $Ri$ increase at a stable value of $Ri$. It is also seen from this Figure 4.18; average fluid temperature rises steadily with rising value of    when $\Delta$ is kept $Ri$ constant.
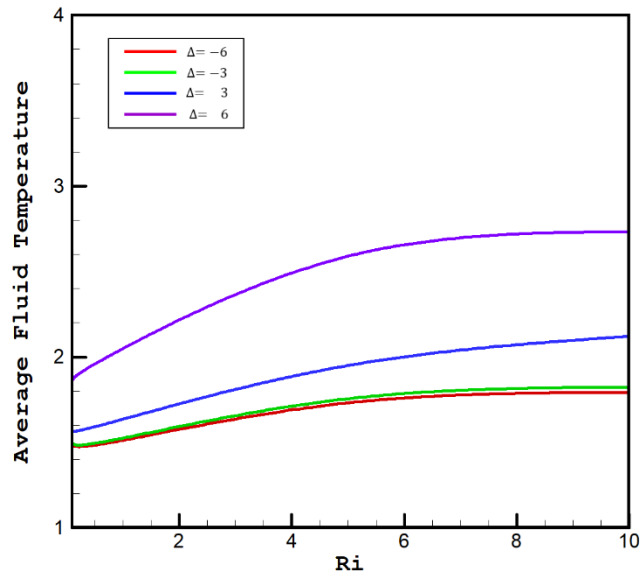
**Figure** 4.**18:** Variation of the average fluid temperature against $Ri$ on the bottom heated wall for selected value $\varDelta$ while $Pr = 0.70, \lambda = 1, Ha = 20, Re = 100$.

Table 4.1 - 4.2 express the values of the average Nusselt number and average fluid temperature respectively for assumed parameters including $\varDelta, Re, Ha, Ri$ and $Pr$ respectively. The numerical outcome indicates that the average Nusselt number expands with expanding the value of $Ri$ and average fluid temperature increases with augmenting the value of $Ri$. Which indicates that with an enlargement in Richardson number heat transfer is enriched.

## 4.5 EFFECT OF UNDULATIONS

In this section, results of the numerical investigation of the effect of undulations on MHD mixed convection heattransfer in presence of heat generation or absorption in a lid-driven cavity are numerically presented. The results have been obtained for the undulation $\lambda = 1, 2$ and 3. The results of this parametric study are shown in Figure 4.19- 4.24.

### 4.5.1 Effect of undulations for heat absorption $(\varDelta = -6)$

The effects of undulation $\lambda = 1, 2$ and 3 on streamlines and isotherms for the present configuration at $Ha = 20, Pr = 0.70, Re = 10^2, Gr = 10^4$ $A = 0.1$ and $\varDelta = -6$ has been demonstrated in Figure 4.19 (a)–(b) in terms of dimensionless velocity profiles. From Figure 4.19(a), it is seen that when $\lambda = 1$ the strength of buoyancy force inside the cavity is significant and two vortices appear inside thecavity which one is major vortex and another one is a minor vortex with one cell. Again, when $\lambda = 2$ the flow structure is similar to $\lambda = 1$.

**Figure 4.19:** Effect of undulation on (a) streamlines and (b) isotherms for $Pr = 0.70, Ha = 20, Re = 10^2, Gr = 10^4, Ri = 1$ and $\Delta = -6$.

Further again when Reynold's number increases to $\lambda = 2$, the strength of the buoyancy force is more significant and two vortices appear. The physical fact behind it's that the greater effect of the undulation increases the buoyancy force to influence the flow field.

On the other hand, in Figure 4.19(b), isotherms are distributed near the bottom wall as it was isothermally heated. Moreover, it occupies the half of the cavity and some isotherms are also concentrated with the centered ellipse as it was heat absorbed. For $\lambda = 2$ and $3$ the vertical heat gradient takes part near the left wall. In addition, the isotherms are effectively close toward the hot wall as $\lambda$ is increased. At each increment in $\lambda$, there is a clear changed in isotherms distribution.

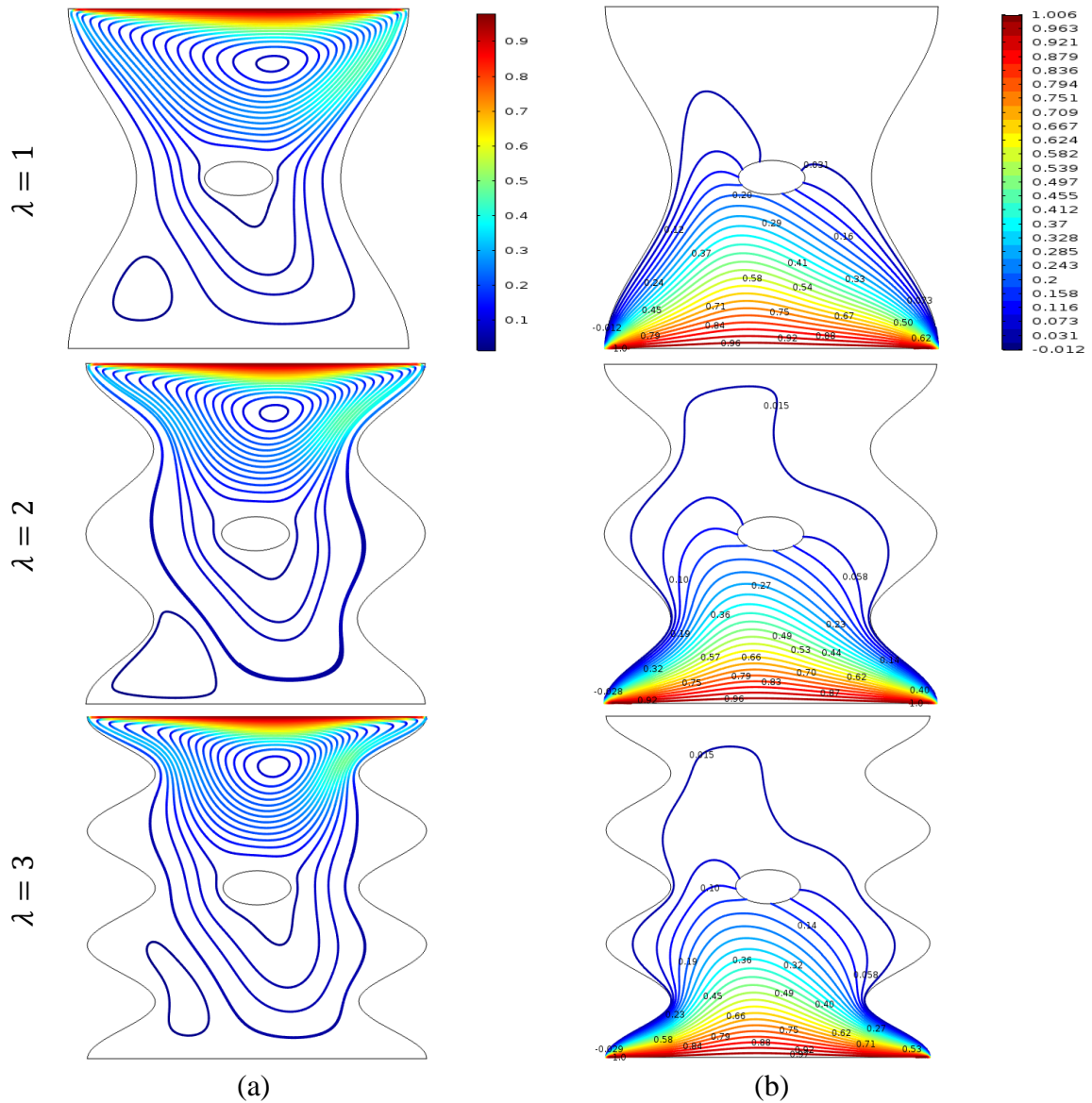**4.5.2 Effect of undulations for heat absorption** ($\Delta = -3$)



**Figure4.20:** Effect of undulation on (a) streamlines and (b) isotherms for $Pr = 0.70, Ha = 20, Re = 10^2, Gr = 10^4, Ri = 1 \ and \ \Delta = -3$.

The effects of undulation $\lambda = 1, 2$ and $3$ on streamlines and isotherms for the present configuration at $Ha = 20, Pr = 0.70, Re = 10^2, Gr = 10^4 \ A = 0.1$ and $\Delta = -3$ has been demonstrated in Figure 4.20-(a)–(b) in terms of dimensionless velocity profiles.

From Figure 4.20(a), it is seen that when $\lambda = 1$ the strength of buoyancy force inside the cavity is significant and two vortices appear inside thecavity which one is major vortex and another one is a minor vortex with one cell. Again, when $\lambda = 2$ there is only one vortex inside the cavity which covered half of the cavity. Further again when Reynold's number increases to $\lambda = 2$, two vortices appear. The physical fact behind it's that the minor effect of the undulation in this case.

On the other hand, in Figure 4.20(b), isotherms are clustered near the bottom wall as it was isothermally heated. Moreover, it occupies the half of the cavity and some isotherms are also concentrated with the centered ellipse as it was heat absorbed. For $\lambda = 2 \,\&\, 3$ the vertical distortion of isotherm counters take part in the left cold wall. In addition, the isotherms are effectively close toward the hot wall as $\lambda$ is increased. At each increment in $\lambda$, there is a clear changed in isotherms distribution compared to previous one.

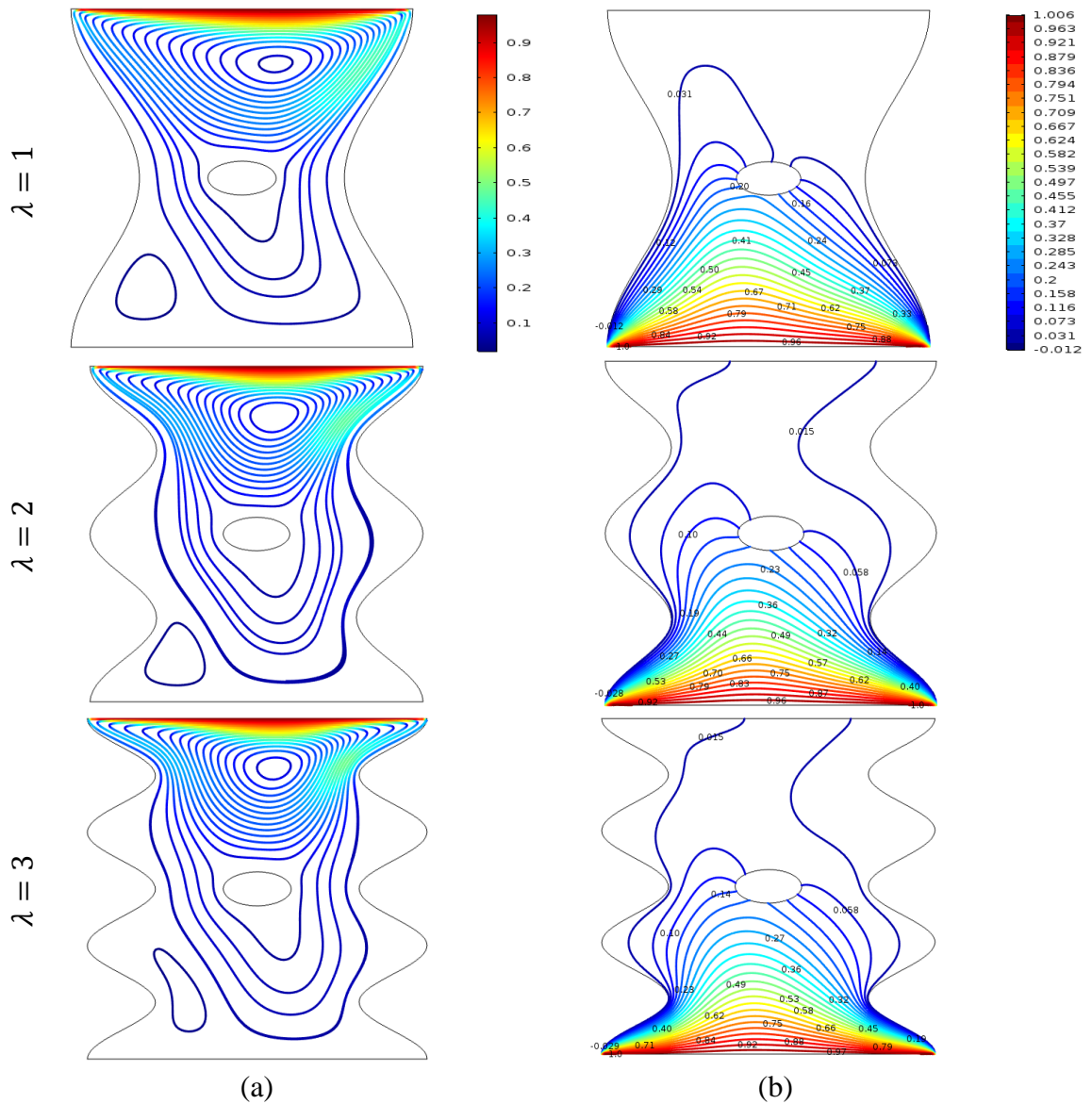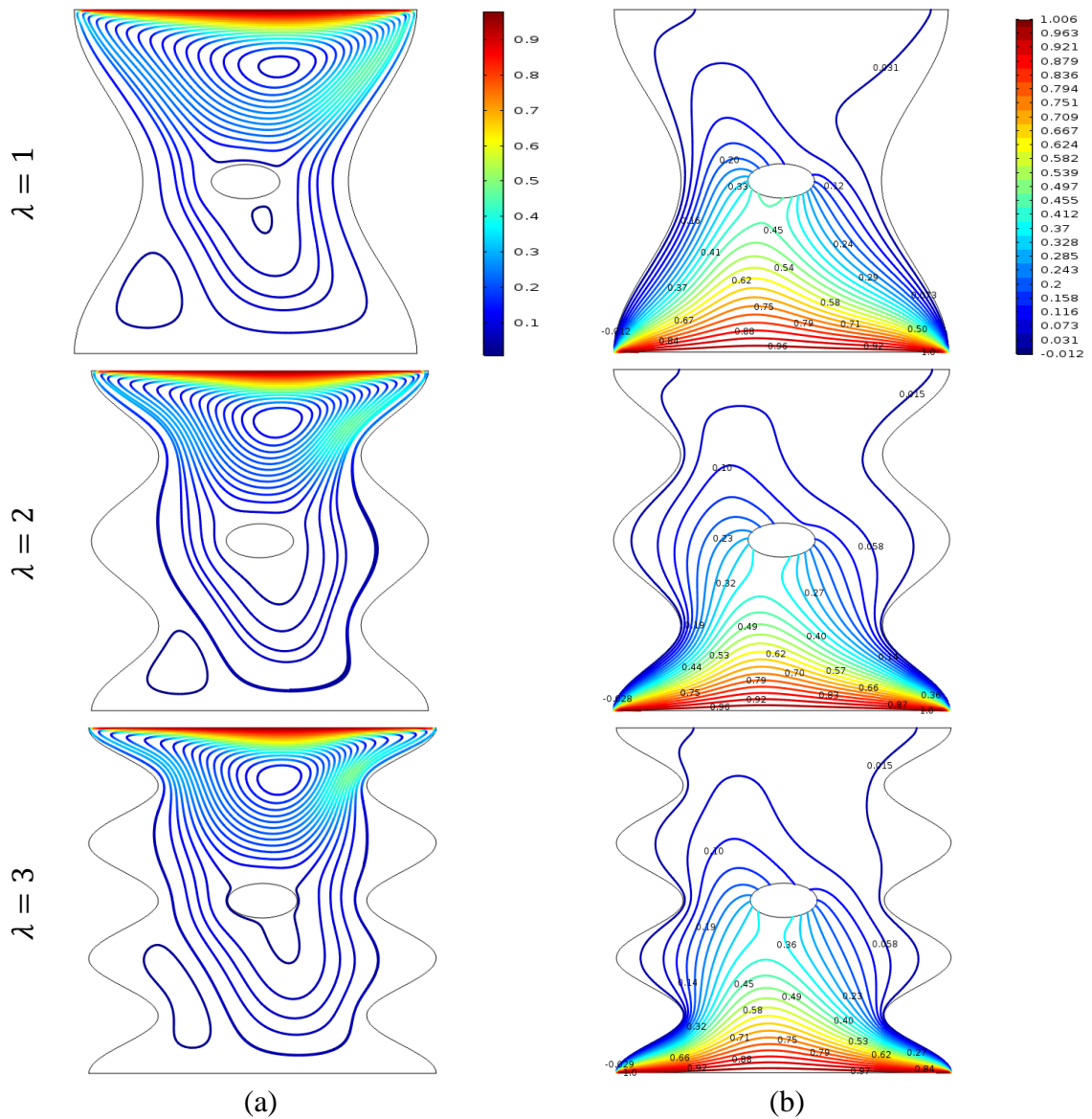### 4.5.3 Effect of undulations for heat generation ($\Delta = 3$)



Figure 4.21: Effect of undulation on (a) streamlines and (b) isotherms for $Pr = 0.70, Ha = 20, Re = 10^2, Gr = 10^4, Ri = 1 \; and \; \Delta = 3$.

The influence of undulation $\lambda = 1, 2$ and $3$ on streamlines and isotherms for the present configuration at $Ha = 20, Pr = 0.70, Re = 10^2, Gr = 10^4$ $A = 0.1$ and $\Delta = -6$ has been demonstrated in Figure 4.21(a)–(b), in terms of dimensionless velocity profiles. From Figure 4.21(a), it is seen that when $\lambda = 1$ the strength of buoyancy force inside the cavity is significant and two vortices appear inside the cavity which one is major vortex and another one is a minor vortex with one cell. Again, when $\lambda = 2,3$ the flow structure is similar to $\lambda = 1$ but in case $\lambda = 2$, the streamline counter's distance of the primary vortex is minimum. Further again when undulation increases to $\lambda = 3$, the streamline counter's distance of the primary vortex increase. The physical fact behind it's that the minor effect of the undulation increases the buoyancy force to influence the flow field.

The isotherm patterns are quite similar for $\lambda = 1, 2$ and $3$ (see Figure 4.21(b)). The contour lines are distributed in the whole cavity. Heat transfer becomes higher and thus the only one or two parallel distribution of isotherm contours breaks up and is distorted throughout the cavity. This distortion in the isotherm contours indicates more significant difference for undulation's variation than previous cases.

### 4.5.4 Effect of undulations for heat generation ($\Delta = 6$)

The impacts of undulation $\lambda = 1, 2$ and $3$ in presence of heat generation $\Delta = 6$ on streamlines and isotherms for the present configuration at $Ha = 20, Pr = 0.70, Re = 10^2, Gr = 10^4, Ri = 1$ and $A = 0.1$ has been presented in Figure 4.22(a)–(b). The changes due to undulations variation in streamlines is observed in Figure 4.22(a). It is seen that when $\lambda = 1$ two vortices appear inside the cavity which one is major vortex and another one minor vortices with one cell. Again, when $\lambda = 2$ the flow structure includes a primary and a secondary vortex inside the cavity. Further again when undulation increases to $\lambda = 3$, the strength of the buoyancy force is more significant and two vortices appear with more contour. The physical fact behind it's that the greater effect of the undulation increases the buoyancy force to influence the flow field.

The effect undulation variation in case of heat generation $\Delta = 6$ has a great impact on isotherms. From Figure 4.22(b), we observed that isotherms are distributed entire the cavity with distortion of some isotherms counter for $\lambda = 1, 2$ and $3$. With the increase of undulation number, the distortion is also increased. The physical fact is at each increment in $\lambda$, there is a greater impact in isotherms distribution compared to previous one.
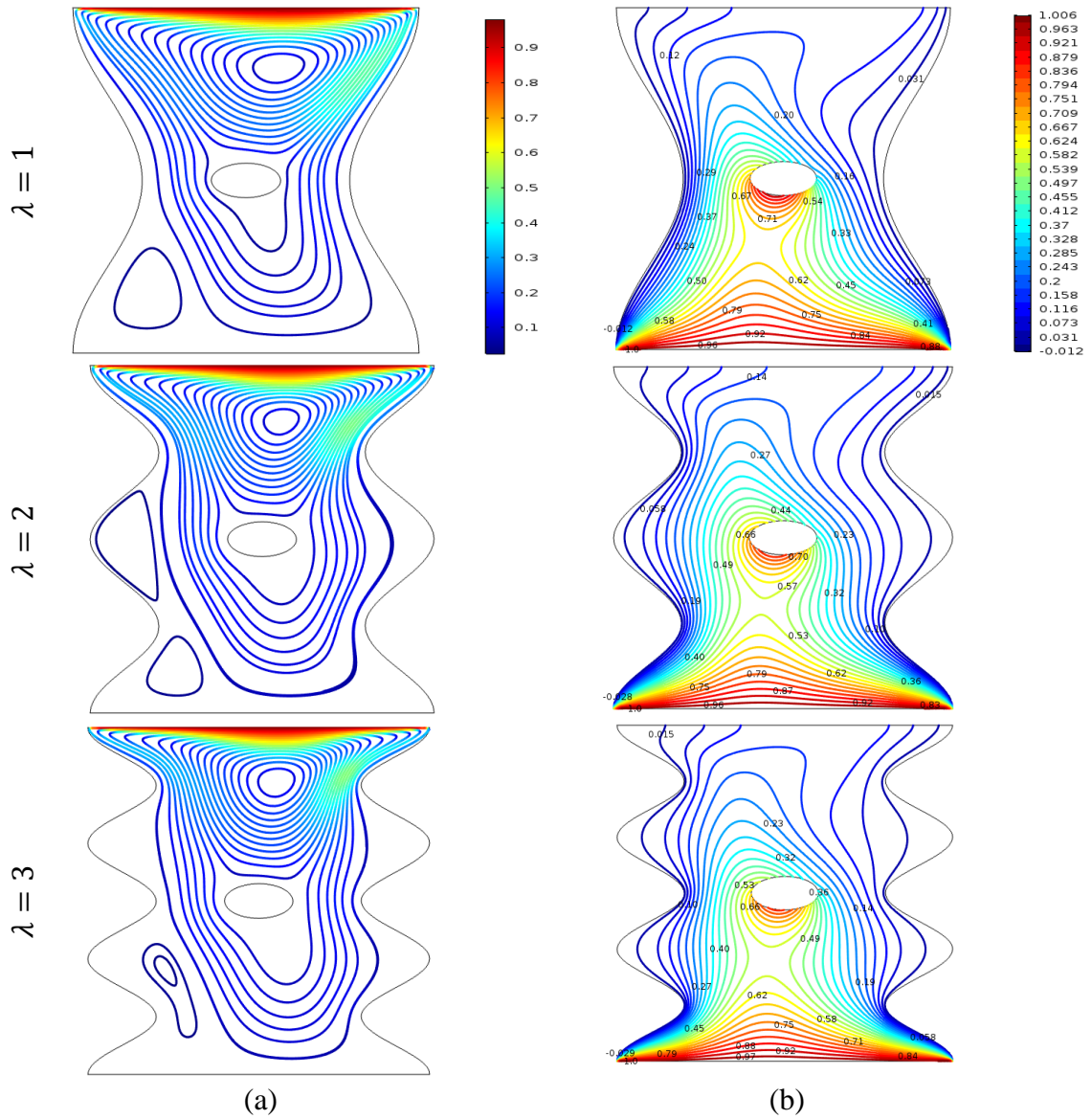
**Figure 4.22:** Effect of undulation on (a) streamlines and (b) isotherms for $Pr = 0.70, Ha = 20, Re = 10^2, Gr = 10^4 \ and \ \Delta = 6$.

### 4.5.5 Heat Transfer Rates

In this section, results of the numerical investigation of mixed convection heattransfer in presence of magnetic field in a lid-driven wavy cavity having vertical fin are numerically presented. The average Nusselt number versus undulation and heat transfer rates are shown in Figure 4.23-4.24 and heat transfer rates Table 4.7-4.8 given below.

**Table 4.7:** Numerical values of average Nusselt number against $\Delta$ bottom heated wall on selected value of undulation while $Pr = 0.70, Ha = 20, Re = 10^2, Gr = 10^4$.

| $\Delta$ | Average Nusselt Number | | |
|---|---|---|---|
| | $\lambda = 1$ | $\lambda = 2$ | $\lambda = 3$ |
| -6 | 6.4419 | 8.0681 | 10.7073 |
| -3 | 6.4356 | 8.0620 | 10.7013 |
| 3 | 6.4236 | 8.0511 | 10.6669 |
| 6 | 6.3982 | 8.0286 | 10.5937 |

Figure 4.23, illustrate that the average Nusselt number ($Nu_{av}$) versus $\Delta$ along the heated bottom wall for various undulation while the value of the remaining parameters is kept fixed. It can beseen from this Figure, the average Nusselt number increases when the value of the undulation number increases. At a constant undulation, with an increase $\Delta$ the average Nusselt number decreased.

**Figure 4.23:** Variation of the average Nusselt number against $\Delta$ for selected value of undulation while $Pr = 0.70, Ha = 20, Re = 10^2, Gr = 10^4$.
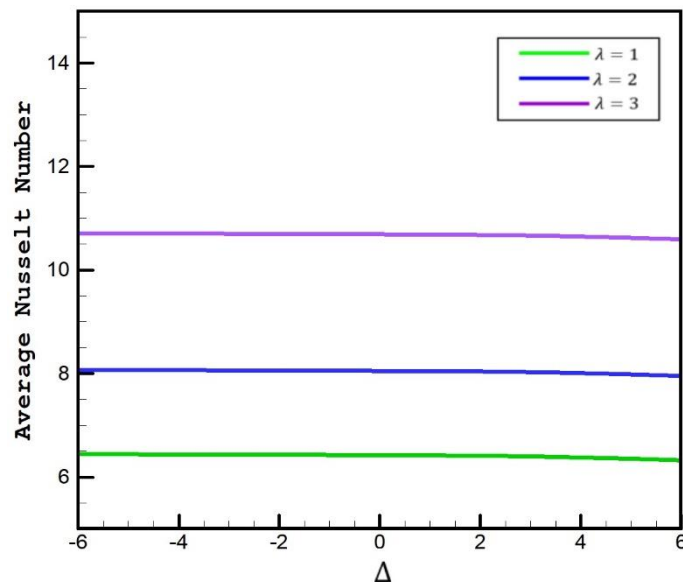


Figure 4.24, illustrate that the average fluid temperature ($\theta_{av}$) versus $\Delta$ for various values of ($\lambda$) while the value undulation of the remaining parameters is kept constant. It can be seen from this figure; average fluid temperature increases when the value of $\Delta$ increases at constant $\lambda$. At a constant undulation, with an increase in $\Delta$ the average fluid temperature increases except in case of $\Delta = 6$.

**Table 4.8:** Numerical values of average fluid temperature against $\varDelta$ for selected value of undulation while $Pr = 0.70, Ha = 20, Re = 10^2, Gr = 10^4$.

| $\Delta$ | Average Fluid Temperature | | |
|---|---|---|---|
| | $\lambda = 1$ | $\lambda = 2$ | $\lambda = 3$ |
| -6 | 1.5124 | 1.5027 | 1.5216 |
| -3 | 1.5255 | 1.5171 | 1.5350 |
| 3 | 1.6355 | 1.6364 | 1.6444 |
| 6 | 2.0491 | 2.1512 | 2.0950 |
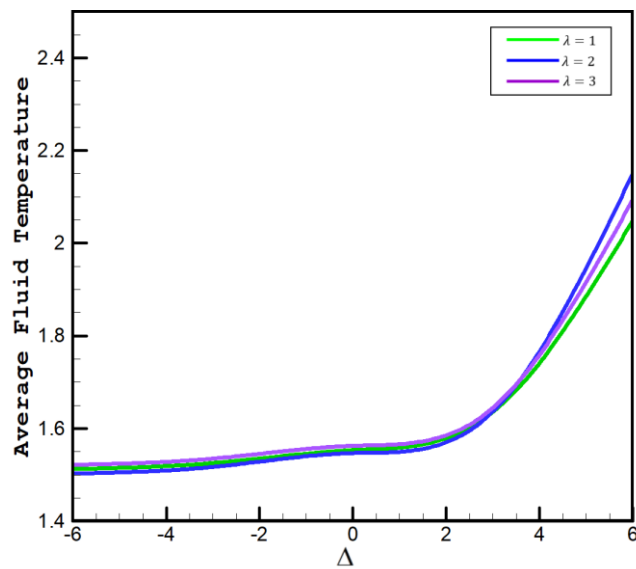


**Figure 4.24:** Variation of the average fluid temperature against $\Delta$ for selected value of undulation while $Pr = 0.70, Ha = 20, Re = 10^2, Gr = 10^4$.

Table 4.7 - 4.8, represent the values of the average Nusselt number and average fluid temperature respectively for considered parameters including $\varDelta, Re\ Gr$ and $Pr$ respectively. Both the numerical result indicates that the average Nusseltnumber and average fluid temperature increases with increasing the value of $\lambda$. At a constant $\lambda$, with an increase in $\varDelta$ average fluid temperature is enhanced but average Nusselt number is decreased.

## 5.1 INTRODUCTION

Mixed convection in a lid-driven cavity heated from the bottom side under the influence of the applied magnetic force and internal heat absorption or generation having variable undulation has been investigated numerically. The results are presented for flow and thermal fields as well as heat transfer for the enclosure subject to a constant hot temperature at the bottom wall of the cavity while the remaining top wall is kept adiabatic and the other two sidewalls are kept at a cold temperature. The finite element method is used to solve governing equations. Comparisons with the beforehand published work are performed and found to be in excellent agreement. The influences of Reynolds number, the Grashof number, the undulations and heat absorption or generation have been reported. The various ideas and results have been discussed in detail in the relevant chapters of the thesis. In the present chapter, an attempt is made to summarize the concepts presented and results obtained in the work reported already. A section on the scope of further work on associated fields of investigation is also included.

## 5.2 SUMMARY OF THE MAJOR OUTCOMES

The effect of $Re$, effect of $Gr$, effect of $Ri$ and effect of undulations when Prandtl number is chosen as $Pr = 0.70$ are considered in this study.

The following main concluding remarks are drawn from the present study:

i. For heat absorption to generation, the maximum increase of heat transfer performance was found to be 3.8% at $Re = 10^3$.

ii. At $Gr = 10^5$ heat transfer performance and average fluid temperature increased $3.5\%$ $and$ 7.8% respectively under the influence of heat absorption and generation.

iii. It was observed that due to heat absorption and generation the maximum enhancement in the average fluid temperature was $7.8\%$ for $Ri = 10$.

iv. In presence of heat absorption and generation, the optimum increase in average fluid temperature was 5.4% for $\lambda = 2$.

**5.3 FUTURE PLANS**

The following can be put forward for the further works as follow-ups of the present research as.

   i. Double diffusive mixed convection can be analyzed through including the governing equation of concentration conservation.

  ii. Investigation can be performed by using magnetic fluid instead of electrically conducting fluid within the porous medium and changing the boundary conditions of the cavity's walls.

 iii. The study can be extended for turbulent flow using different fluids, different thermal boundary conditions such as constant heat flux or radiation and unsteady flow.

  iv. Only two-dimensional fluid flow and heat transfer has been analyzed in this thesis. So, this deliberation may be extended to three-dimensional analyses to investigate the effects of parameters on flow fields and heat transfer in cavities.

   v. The study can be extended by choosing different shapes of the cavity.

  vi. The study can be extended for Nano-fluids.

## REFERENCES

[1]     K. D. Hagen, "Heat Transfer with Applications", 1st ed., Prentice-Hall International, 1999.

[2]     Y. A. Çengel and J. M. Cimbala, "Fluid Mechanics: Fundamentals and Applications", 3rd ed., McGraw-Hill, 2013.

[3]     J. A. Shercliff, "A Textbook of Magnetohydrodynamics", 1st ed., Pergamon Press, UK, 1965.

[4]     Çengel and Yunus, "Heat Transfer: A practical approach", 2nd ed., Boston: McGraw-Hill, 2003.

[5]     Cengel Y. A., "Heat and mass transfer", Third ed., Tata McGraw Hill., 2007.

[6]     S. V. Patankar, "Numerical Heat Transfer and Fluid Flows", 1st ed. Hemisphere Publishing Corporation, U. S.A, 1980.

[7]     J. H. Ferziger and M. Perić, "Computational Methods for Fluid Dynamics", 3rd ed. Springer, 2002.

[8]     M. A. Ismael, I. Pop and A. J. Chamkha, "Mixed Convection in a Lid-Driven Square Cavity with Partial Slip", Int. J. Ther. Sci., Vol. 82, pp. 47-61, 2014.

[9]     S. Mahmud, P. K. Das, N. Hyder, A. K. M. S. Islam, "Free Convection in an Enclosure with Vertical Wavy Walls", Int. J. Ther. Sci., Vol. 41, pp. 440-446, 2002.

[10]    E. Abu-Nada and A. J. Chamkha, "Mixed Convection Flow of a Nanofluid in a Lid-Driven Cavity with a Wavy Wall", Int. Comm. in Heat and Mass Transfer, Vol. 57, pp. 36-47, 2014.

[11]    L. K. Saha, M. C. Somadder and K. M. S. Uddin, "Mixed Convection Heat Transfer in a Lid Driven Cavity with Wavy Bottom Surface", American J. App. Math., Vol. 1(5), pp. 92-101, 2013.

[12]    M. M. Rahman, M. A. Alim, M. A. H. Mamun, M. K. Chowdhury and A. K. M. S. Islam, "Numerical Study of Opposing Mixed Convection in a Vented Enclosure", ARPN J. of Eng. Appl. Sci., Vol. 2, No. 2, pp. 25-36, 2007.

[13]    M. F. A. Asad, M. N. Alam, H. Ahmad, M.M.A. Sarker, M.D. Alsulami, and K. A. Gepreel, "Impact of a closed space rectangular heat source on natural convective flow through triangular cavity", Result Phys., Vol. 23, pp. 1-7, 2021.

[14]  S. Singh and M. A. R. Sharif, "Mixed convective cooling of a rectangular cavity with inlet and exit openings on differentially heated side walls", Numer. Heat Trans., Vol. 44, pp. 233–253, 2003.

[15]  M.K. Moallemi and K.S. Jang, "Prandtl number effects on laminar mixed convection heat transfer in lid-driven cavity", Int. J. Heat Mass Trans., Vol. 35, pp. 1881–1892, 1992.

[16]  C. Gau, Y. C. Jeng and C. G. Liu, "An experimental study on mixed convection in a horizontal rectangular channel heated from a side", ASME J. Heat Trans., Vol. 122, pp. 701–707, 2000.

[17]  T.H. Hsu and S. G. Wang, "Mixed convection in a rectangular enclosure with discrete heat sources", Numer. Heat Trans., Part A, Vol. 38, pp. 627-652, 2000.

[18]  A. A. Amiri, K. Khanafer, J. Bull and I. Pop, "Effect of sinusoidal wavy bottom surface on mixed convection heat transfer in a lid-driven cavity", Int. J. Heat Mass Trans., Vol. 50, pp. 1771–1780, 2007.

[19]  Q. Wang and Y. Jaluria, "Instability and heat transfer in mixed convection flow in a horizontal duct with discrete heat sources", Numer. Heat Trans., Vol. 42, pp. 445-463, 2002.

[20]  H. F. Oztop, "Influence of exit opening location on mixed convection in a channel with volumetric heat sources", Int. Comm. Heat Mass Trans., Vol. 37, pp. 410-415, 2011.

[21]  A. B. Nakhi and A. J. Chamkha, "Conjugate Natural Convection in a Square Enclosure with Inclined Thin Fin of Arbitrary Length", Int. J. Therm. Sci., Vol. 46, pp. 467-478, 2007.

[22]  H. Sertel and K. Bilen, "The effect of using sinusoidal profile in fins on thermal performance", Int. J. Heat Tech., Vol. 37, pp. 541-750, 2019.

[23]  A. Elatar, M. A. Teamah and M. A. Hassab, "Numerical study of laminar natural convection inside square enclosure with single horizontal fin", Int. J. Therm. Sci., Vol. 99, pp. 41-51, 2016.

[24]  M. F. Asad, M. J. H. Munshi, R. K. Bhowmik and M. A. Sarker, "Numerical Investigation of Natural Convection Flow in a Hexagonal Enclosure Having Vertical Fin", J. Scien. Res., Vol. 11, pp. 173-183, 2019.

[25]  D. Angirasa, "Mixed convection in a vented enclosure with isothermal vertical surface", Fluid Dyn. Res., Vol. 26, pp. 219-233, 2000.

[26] C.H. Cheng and C.L. Chen, "Numerical study of effects of inclination on buoyancy induced flow oscillation in a lid-driven arc-shaped cavity", Numer. Heat Trans., Vol. 48, pp. 77–97, 2005.

[27] Md.Nur Alam, and C Tunç, "An analytical method for solving exact solutions of the nonlinear Bogoyavlenskii equation and the nonlinear diffusive predator–prey system", Alex. Eng. J., Vol. 11, pp.152–161, 2016.

[28] H. Ahmad, A. R. Seadawy, T. A. Khan, P. Thounthong, "Analytic approximate solutions for some nonlinear Parabolic dynamical wave equations", J. Taibah Univ. Sci., Vol. 14(1), pp. 346–358, 2020.

[29] C. Taylor and P. Hood, "A numerical solution of the Navier-Stokes equations using the finite element technique." Int. J. of Comp. Fluids, Vol.1, pp.73-89, 1973.

[30] K. Javaherdeh, M. Moslemi, and Shahbazi, "Natural convection of nanofluid in a wavy cavity in the presence of magnetic field on variable heat surface temperature", J. Mech. Sci. Tech., Vol. 31, pp. 1937-1945, 2017.

[31] A. Malleswaran and S. Sivasankaran, "Numerical Simulation on MHD Mixed Convection in a Lid Driven Cavity with Corner Heaters", Int. J App. Fluid Mech., Vol. 9(1), pp. 311-319, 2016.

[32] H. R. Ashorynejad and A. Shahriari, "MHD Natural Convection of Hybrid Nanofluid in an Open Wavy Cavity", Results Phys., Vol. 9, pp. 440-455, 2018.

[33] H. F. Öztop, A. Sakhrieh, E. Abu-Nada and K. A. Salem, "Mixed Convection of MHD Flow in Nanofluid Filled and Partially Heated Wavy Walled Lid-Driven Enclosure", Int. Comm. in Heat Mass Trans., Vol. 86, pp. 42-51, 2017.

[34] K. M. Gangawane, H. F. Oztop and M. A. Ali, "Mixed Convection in a Lid-Driven Cavity Containing Triangular Block with Constant Heat flux: Effect of Location of Block", Int. J. Mech, Sci., Vol. 152, pp. 492-511, 2019.

[35] L. K. Saha, K. M. S. Uddin and M. A. Taher, "Effect of internal heat generation or absorption on MHD mixed convection flow in a lid driven cavity", American J. Appl. Math., Vol. 3, pp. 20-29, 2015.

[36] S. Pervin and R. Nasrin, "Analysis of the flow and heat transfer characteristics for MHD free convection in an enclosure with a heated obstacle", Nonl. Analy. Mod. Cont., Vol. 16, pp. 89-99, 2011.

[37]  A. J. Chamkha, "Hydromagnetic combined convection flow in a vertical lid-driven cavity with internal heat generation or absorption", Numer. Heat Trans., Part A, Vol. 41, pp. 529-546, 2002.

[38]  S. H. Mahmud, S. Tasnim, and M. A. H. Mamun, "Thermodynamic analysis of mixed convection in a channel with transverse hydromagnetic effect", Int. J. of Therm. Sci., Vol. 42, pp. 731-740, 2003.

[39]  N. A. Bakar, A. Karimipour and R. Roslan "Effect of Magnetic Field on Mixed Convection Heat   Transfer in a Lid-Driven Square Cavity", J. Thermo., Vol. 2016, pp. 1-14, 2016.

[40]  T. Basak, S. Roy, P. K. Sharma and I. Pop, "Analysis of mixed convection flows within a square cavity with uniform and non-uniform heating of bottom wall", Int. J. Therm. Sci., Vol. 48, pp. 891-912, 2009.

[41]  M. M. Ali, M. A. Alim and S. S. Ahmed, "Magneto-hydrodynamic mixed convection flow in a hexagonal enclosure", Procedia Eng., Vol. 194, pp. 479 – 486, 2017.

[42]  B. Xu, B. Q. Li, and D. E. Stock, "An experimental study of thermally induced convection of molten gallium in magnetic fields", Int. J. Heat Mass Trans., Vol. 49, pp. 2009–2019, 2006.

[43]  O. Manca, S. Nardini, K. Khanafer, and K. Vafai, "Effect of heated wall position on mixed convection in a channel with an open cavity", Numer. Heat Trans., Vol. 43, pp. 259–282, 2003.

[44]  H. T. Cheong, S. Sivasankaran, M. Bhuvaneswari, "Natural convection in a wavy porous cavity with sinusoidal heating and internal heat generation", Int. J. Num. Meth. Heat Fluid Flow, Vol.27 (2), pp.287-309, 2017.

[45]  A. Chattopadhyay, S. K Pandit, S. S. Sarma, I. Pop, "Mixed convection in a double lid-driven sinusoidally heated porous cavity", Int. J. Heat Mass Trans, Vol.93, pp.361-378, 2016.